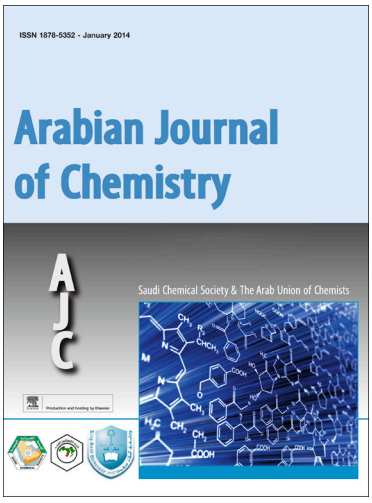

Original article

Hierarchical zinc aluminate 3D nanostructures, synthesized by bio-inspired ultrasound assisted sonochemical route: Display and dosimetry applications

F. Femila Komahal, H. Nagabhushana, G.P. Darshan, B. Daruka Prasad

PII: S1878-5352(17)30132-6
DOI: http://dx.doi.org/10.1016/j.arabjc.2017.07.002
Reference: ARABJC 2114

To appear in: *Arabian Journal of Chemistry*

Received Date: 30 March 2017
Accepted Date: 2 July 2017

Please cite this article as: F. Femila Komahal, H. Nagabhushana, G.P. Darshan, B. Daruka Prasad, Hierarchical zinc aluminate 3D nanostructures, synthesized by bio-inspired ultrasound assisted sonochemical route: Display and dosimetry applications, *Arabian Journal of Chemistry* (2017), doi: http://dx.doi.org/10.1016/j.arabjc.2017.07.002

Hierarchical zinc aluminate 3D nanostructures, synthesized by bio-inspired ultrasound assisted sonochemical route: Display and dosimetry applications

F. Femila Komahal[1, 2], H. Nagabhushana[3, *], G.P. Darshan[4], B. Daruka Prasad[5]

[1]Department of Physics, Government Science College, NT Road, Bangalore-560 001, India

[2]Research and Development Center, Bharathiar University, Coimbatore- 641 046, India

[3]Prof. C.N.R. Rao Centre for Advanced Materials Research, Tumkur University, Tumkur- 572 103, India

[4]Department of Physics, Acharya Institute of Graduate Studies, Bangalore- 560 107, India

[5]Department of Physics, BMS Institute of Technology, VTU- Belagavi, Bangalore -560 064, India

ABSTRACT

$ZnAl_2O_4:Tb^{3+}$ (0.25 - 5 mol %) nanophosphor were synthesized by ultrasound assisted sonochemical route using bio-sacrificial *Aloe Vera* (*A.V.*) gel as a template. The effect of sonication time, *A.V.* gel concentration, pH value, sonication power and temperature on the morphologies of the prepared samples were systematically explored and discussed. Probable formation mechanism for various morphologies of $ZnAl_2O_4:Tb^{3+}$ nanophosphor was discussed. Structural and luminescence properties of the obtained samples were thoroughly investigated. Rietveld refinement of the prepared samples exhibit cubic structure with $Fd\bar{3}m$ space group. Thermoluminescence (TL) glow curves exhibit a well resolved glow peak at ~ 197 °C. TL intensity was found to increase linearly up to 1 kGy and thereafter it shows sub-linear behavior with increase of dose which indicates that the present phosphor was quite useful for TL dosimetry. Kinetic parameters related with the glow peaks were estimated by different methods. Photoluminescence (PL) spectra shows the characteristic Tb^{3+} ion peaks at ~ 488 nm, 542 nm, 584 nm and 622 nm corresponding to $^5D_4 \rightarrow {}^7F_J$ (J = 3, 4, 5 and 6) transitions respectively. The chromaticity co-ordinates of all the phosphors were well located in green region. Therefore, the present phosphor was quite useful as green component of white light- emitting diodes.

KEYWORDS: Bio - inspired synthesis; nanostructures; Photoluminescence;

Thermoluminescence; Judd-Ofelt analysis

*Corresponding Author: E-mail address: bhushanvlc@gmail.com (Dr. H. Nagabhushana)

1. Introduction

Thermoluminescence dosimetry (TLD) has an application in personnel and environmental dosimetry, radiation therapy, ageing of archaeological and geological samples etc. Thermoluminescence (TL) property play an vital role in acquiring the data of the kinetic parameters such as trap depth (E), frequency factor (s) and order of kinetics of the traps present in the solids (Kitis et al., 1994; Kortov et al., 1994). Further, TL depends on the numerous parameters such as the energy band gap, fabrication route, crystallite size, lattice defects and largely the effects of impurities / dopants present in the materials (Premkumar et al., 2013a). To control the TL response, different types of materials both in bulk and nano were prepared and well discussed in the literature (Premkumar et al., 2014b; Sunitha et al., 2014; Sunitha et al., 2013b, Burda et al., 2005). Presently nanophosphors with different morphologies have attracted several researches in material science, particularly in the field of luminescence. Recent literature evident that TL studies of various luminescent nanomaterials showed better potentiality when compared to the conventional microcrystalline phosphors towards the dosimetry of ionizing radiations (Shivaram et al., 2013; Premkumar et al., 2013c; Hari Krishna et al., 2014). Therefore, in order to obtain efficient TLD phosphor, synthesis method plays a key role in engineering the crystallite size, shape and surface area of the phosphor (Vossmeyer et al., 1994; Dimitrijevic at al., 2007).

Till date numerous synthesis routes have been used for prepare $ZnAl_2O_4$ powders, such as solid-state, co-precipitation, hydrothermal, sol-gel, solution combustion method etc. (Geeta Rani., 2017; Rui Yang et al., 2017; Pushpa Kumari et al., 2016; Premkumar et al., 2013c; Mithlesh Kumar et al., 2015). However, the majority of these methods need sophisticated equipment and complicated experimental procedures. Therefore, it is still a challenge to research community to explore a simple, fast, environmental friendly and cost effective synthesis method to avoid highly toxic chemicals and utilization of more energy

(Lou et al., 2004; Strek et al., 2000; Cheng et al., 2006; Rusu et al., 2009). Ultrasound assisted sonochemical synthesis method using plant extracts as surfactants have showed the better path towards the same (Venkataravanappa et al., 2016a, Ekaterina et al., 2013). The main advantage of this method was to reduce the calcination temperature, selection of new solvents and vary the experimental condtions to get the required shape, size and surface area of the product and in shorter duration. When ultrasound was passed through a liquid, successive rarefaction and compression of waves at a very high temperature and pressure will create disintegration and collapsing of bubbles was sufficient to modify the materials properties (Jin Ho Bang et al., 2010).

As a green revolution, use of naturally existing contents as surfactants for the synthesis of nanomaterials is of more advantageous. Therefore, the bio- inspired synthesis of nanostructures is highly proficient and cost-effective (Sankar et al., 2014). Recently, several extracts from the plants were used to fabricate superstructures of oxides, silicates, sulphides, fluorides and etc. (Suresh et al., 2017; Venkataravanappa et al., 2016b; Amith Yadav et al., 2017; Darshan et al., 2016; Dhanalakshmi et al., 2017).

Aloe Vera (*A.V.*) was an eternal juicy plant grows in dry and hot climatic conditions has been used for multifunctional applications such as antiprotozoal, UV protective, anti-inflammatory, wound- healing properties etc. (Reynolds et al., 1999; Shin et al., 1997; Umano et al., 1999; Saccu et al., 2001). In addition, it have been reported that the employ of *A.V.* gel was found to be highly useful for the synthesis of various shapes of nano/micro structures because of its environment friendly, non-polluting compatible solvent system, eco-friendly reducing agent and a non-hazardous gelling agent for stabilizing the nanostructures (Chandran et al., 2006; Maensiri et al., 2008; Phumying et al., 2013; Klinkaewnarong et al., 2010; Laokul et al., 2009; Laokul et al., 2011, Visinescu et al., 2011; Varma et al., 2012; Boudreau et al., 2006).

Over the past few decades, many researchers have been focused on the fabrication of efficient luminescent nanophosphors due to its wide range of applications in display, solar cells, catalysts, sensors etc. (Thinesh Kumar et al., 2012; Ciupina et al., 2004; der Laag et al., 2004). Among them, nano zinc aluminate ($ZnAl_2O_4$) has been found to be an efficient host material with a wide optical band gap (3.8 eV), possibility of generating broad band emission and high thermal stability. Due to its transparent and electro conductive properties, it can be used for ultraviolet (UV) photo electronic devices (Ravikumar et al., 2014a).

To the best of our knowledge, this is the first report on the synthesis of $ZnAl_2O_4:Tb^{3+}$ (0.25- 5mol %) nanophosphor using bio-sacrificial *A.V.* gel assisted ultrasonication method. Influence of various experimental parameters on the morphologies of $ZnAl_2O_4$: Tb^{3+} (0.25-5 mol %) nanophosphor was systematically investigated. The TL, photoluminescence (PL) and photometric characteristics of fabricated phosphor were thoroughly studied and discussed.

2. Experimental

2.1. Chemicals and materials

Chemicals used for the synthesis of $ZnAl_2O_4:Tb^{3+}$ nanophosphors were of analytical grade Zinc nitrate [$Zn(NO_2)_3.6H_2O$], Aluminium nitrate [$Al(NO_3)_3.6H_2O$] and Terbium nitrate [$Tb(NO_3)_3.6H_2O$] purchased from sigma Aldrich and were used without further purification. The bio- template self-sacrificial *A.V.* gel extract was collected from the inner gel portion of the *A.V.* leaves which was lightly crushed and ground into thin jelly form and filtered with a fine mesh cotton cloth. The detailed extraction procedure was followed as reported elsewhere (Patel et al., 2013).

2.2. Synthesis

$ZnAl_2O_4$: Tb^{3+} (0.25 - 5 mol %) nanophosphor were synthesized by a bio-template *A.V.* gel assisted ultrasonication method by using intense ultrasound horn of diameter ~ 19 mm, with variable operating frequency. Stoichiometric quantity of zinc nitrate (2.9747 g) and aluminium nitrate (7.5026 g) were dissolved in 100 ml distilled water and homogeneously mixed in a magnetic stirrer to get a uniform solution. Further, the stoichiometric amount of terbium nitrate (0.25 - 5 mol %) as well as different concentration of *A.V.* gel was added to above solution slowly and introduced ultrasound horn into the solution by maintaining the power of ~ 50 W, corresponding to the intensity of ~ 17.6 Wcm^{-2} under ambient air at fixed temperature of 75 °C. The samples of $ZnAl_2O_4$: Tb^{3+} (0.25 - 5 mol %) were prepared by varying ultrasonic time (1 - 6 h). For adjusting different pH values, NaOH was added drop wise in the reaction mixture. The solution was kept undisturbed until a white precipitate was formed. Further, the precipitate was filtered and washed thoroughly by using distilled water and ethanol. The obtained product was dried at 60 °C for 3 h in a vacuum oven. Finally, the product was grinded well into powder form. **Fig.S1.** shows the schematic representation for the synthesis of Tb^{3+} doped $ZnAl_2O_4$ nanophosphor.

2.3. Characterization

Shimadzu X-ray diffractometer (PXRD-7000) using CuK_α radiation (λ=1.541 Å) was used to study the crystalline purity and phase of prepared samples. The *Fullprof* suite programme was used to refine the structural details of sample. Morphology, particle and crystallite sizes were examined by scanning electron (SEM, Hitachi-3000 model) and transmission electron microscopy (TEM, TECNAI F-30 model) respectively. Perkin Elmer spectrometer (Spectrum 1000) was used to study the Fourier transform infrared spectroscopy (FTIR). Excitation and emission spectra of synthesized samples were examined by using Horiba Flurolog-3

Spectroflourimeter. The Nucleonix TLD reader was used to record TL glow peaks by irradiating with γ - rays in the dose range 0.1–6 kGy.

2.4. Theoretical background

Judd-Ofelt (J – O) theory was used to estimate intensity parameters (Ω_2, Ω_4 and Ω_6) from PL emission spectra (Judd, 1962; Ofelt, 1962). These parameters were extensively used to study the structure, bonding and radiative transitions of rare earth (RE) ions in the host matrix. J - O parameters provide the estimated values of radiative transition rates (A_T), radiative lifetime (τ_{rad}), branching ratio $\beta(\psi_J)$ and asymmetric ratio (A_{21}) of the material. From these results, environment around the metal ion and covalency of metal - ligand bonds can be evaluated. The relation between integrated emission intensities of the radiative transitions and emission rates was given by (Som et al., 2014a; Som et al., 2012b);

$$A_{0-j} = \frac{A_{0-2,4}}{A_{0-1}} = \frac{I_{0-2,4}}{I_{0-1}} = \frac{h\upsilon_{0-1}}{h\upsilon_{0-2,4}} \qquad \text{---------- (1)}$$

where $I_{0\text{-}J}$; emission intensity and $h\nu_{0-J}$; energies related to transitions $^5D_0 \rightarrow {}^7F_J$ (J=1, 2, 4) respectively. The radiative transition rate (A_{0-j}) of electric dipole transition in terms of J - O intensity parameters were expressed by the following relation;

$$A_{(0-J)} = \frac{64\pi^4 \vartheta_J{}^3 e^2}{3h(2J+1)C^3} \frac{n(n^2+2)^2}{9} \frac{1}{4\pi\varepsilon_0} \sum_{\lambda=2,4} \Omega_\lambda \left| \left\langle {}^5D_0 \left\| U^{(\lambda)} \right\| {}^7F_J \right\rangle \right|^2 \qquad \text{---------- (2)}$$

where J ; angular momentum quantum number of the initial (final) state of rare earth ions, n ; refractive index of the sample, $\frac{n(n^2+2)^2}{9}$; local field correction factor for the ions in the host medium as a function of refractive index, $\left| \left\langle {}^5D_0 \left\| U^{(\lambda)} \right\| {}^7F_J \right\rangle \right|^2$; squared reduced matrix elements and were independent of chemical environment of Tb^{3+} ions. Eqns. (1) and (2) fitted by least squares fit method to evaluate J - O (Ω_2 and Ω_4) parameters.

The total radiative transition probability (A_T) was achieved by sum of all the radiative rates A_{0-j} for each transition was given by the relation (Som et al., 2014a);

$$A_T = \sum_{J'} A_{J-J'} \quad \text{---------- (3)}$$

The reciprocal of the total radiative transition rate (A_T) gives radiative lifetime (τ_{rad}) of excited level and was given by the relation;

$$\tau_{rad} = \frac{1}{A_T} \quad \text{---------- (4)}$$

The branching ratio $\beta(\psi_J)$ related to the emission from an excited level to its lower level was given by;

$$\beta(\psi_J) = \frac{A(J, J')}{A_T} \quad \text{---------- (5)}$$

3. Results and discussion

Fig.1 shows the SEM micrographs of $ZnAl_2O_4$: Tb^{3+} (3 mol %) nanophosphor synthesized with different ultrasound irradiation time (1-6 h). When ultrasound irradiation time was at ~ 1 h, spike-like structures begin on the surface was observed (**Fig.1 (a)**). When it was increased, small spikes undergo self assembly and growth to form well-defined clear spike like structured with typical widths of ~20–45 μm. The physical phenomenon in this process involves acoustic cavitation. Due to ultrasound irradiation, the formation, growth and collapse of the bubbles happen in the reaction mixture. The solute vapour diffuses volume of the bubble leads to bubble growth. In addition, evaporated water molecules and gas molecules were also incorporated in the bubbles. When the bubble reaches to unstable size, collapse of bubbles will takes place in the reaction mixture. This collapse can generate high temperature ~ 5000 $^{\circ}$C and high pressure ~ 2000 atm in the reaction environment (Suslick et al., 1990). The generation of shock waves and radical can also originated due to bubble

collapse. Moreover, the bubble collapse happened in a very short time, and was favored to very high cooling rate at ~ 10^{11} K/s. Hinder to crystallization and assembly of the product was due to this high cooling rate. This may be the reason for the formation of hierarchical morphology of materials in the presence of ultrasound irradiation at low temperature. The schematic representation for demonstrate the nucleation, growth and collapse of a bubble stimulated by ultrasound irradiation was shown in **Fig.S2.**

Fig. 2 shows the SEM images of $ZnAl_2O_4$: Tb^{3+} (3mol %) nanophosphor with different concentration of *A.V.* (5, 10, 15, 20, 25 and 30 ml) with 5 h of ultrasonic irradiation time. It was evident that, as the concentration of *A.V.* gel increases, the layer formation in structures gradually reduces finally a conversion of layered to bud like structures were obtained. To know the establishment of the layered like morphology, a methodical broad range (from acidic to basic) of pH controlled (5, 7, 9, 11, 12 and 13) experiments were done on $ZnAl_2O_4$: Tb^{3+} (3 mol %) and its influence on the structure/microstructure of prepared superstructures were investigated with 5 h of ultrasonic irradiation time **(Fig. 3)**. SEM studies revealed that the morphology of the products varied significantly by changing pH values from 3 to 8 during mixing of the reactants. When pH is equal to 3 and 4, resulted in the self-assembly of spherical structures, whereas, pH is equal to 5 resulted into the cactus like morphology. We also found that increasing of pH after a certain threshold value (for example pH 9) resulted in total collapse of the layered-like morphology. **Fig.4.** SEM images of $ZnAl_2O_4$: Tb^{3+} (3 mol %) nanophosphor with different sonication power (20, 22, 24 and 26 kHz) with 5 h of ultrasonic irradiation time. The above results evident that the concentration of *A.V.* gel, pH and sonication power plays an important role in tuning the 3D-micro / superstructures of $ZnAl_2O_4$ nanophosphor.

The effect of temperature on morphology of the prepared sample was systematically examined for temperatures 50, 60 and 70 °C in the presence of ultrasound. It was evident

from the images that the flakes orderly stacked side by side to form nacre-like structure when temperature is 50 °C. When temperature increased to 60 °C, groove- like structure was observed. Further, flower-like morphology was observed when temperature was increased to 70 °C **(Fig.5).** To know the effect of ultrasound during the synthesis, mechanical stirring with various time period (1, 2 and 3 h) was applied instead of ultrasound in the presence of 30 ml *A.V.* gel. Interestingly irregular shaped with large agglomerated particles were formed when the stirring time was 1 h (**Fig. 6**). In addition, self assembled particles were observed after 3 h of stirring. The stirring upto 3 h was required for complete precipitation of reaction solution as compared to 1 h ultrasound irradiation. This shows that ultrasound assisted fabrication method requires extremely less time to prepare nanostructures and also it support the effect of cavitation for the formation of well-ordered crystallized nanostructures. A.V. gel contains many varieties of polysaccharides wrapped with protein chains. At the time of stirring, the network of polysaccharides assembles in a complex structured form and then it dissociates leaving behind the trapped nanopartilces. This can be explained by egg-box model as reported elsewhere (Lakshmesh et al 2014, Kavyashree et al 2015, Basavaraj et al 2017).

Depending upon the nature of solvent, reactants (e.g., volatile and non volatile precursors) and vapour pressure, normally the reaction takes place in three different regions. Initially the reaction process may occur in interior part of the cavitation bubbles and bulk solution in case of volatile precursors (e.g., metal carboxylates, water) whereas in non-volatile precursors (metal acetates and metal chlorides), the reaction takes place at interface of cavitation bubbles and the bulk solution. The reaction takes place between the reactant molecules and surviving OH^* or H^* at room temperature in third region. In ultrasound process water pyrolyzed into $OH^*$and H^* radicals and was given below.

$$H_2O \rightarrow H^* + OH^* \qquad \text{---------- (6)}$$

$$H^* + H^* \rightarrow H_2 \quad \text{---------- (7)}$$

$$OH^* + OH^* \rightarrow H_2O_2 \quad \text{---------- (8)}$$

The reaction mechanism for the synthesis of $ZnAl_2O_4$: Tb^{3+} nanophosphor was given below:

$$Zn(NO_2)_3 + Al(NO_3)_3 + 6H_2O \rightarrow Zn(OH)_2 + Al(OH)_4 + 6HCl \quad \text{---------- (9)}$$

$$6HCl + 6NaOH \rightarrow 6NaCl + 6H_2O \quad \text{---------- (10)}$$

$$Zn(OH)_2 + Al(OH)_4 \rightarrow ZnAl_2O_4 + 3H_2O \quad \text{---------- (11)}$$

Therefore, from the above equations it can be observed that ultrasound energy can generate free radicals from the molecules of water and responsible for the formation of $ZnAl_2O_4$: Tb^{3+} nanophosphors at low temperature.

TEM, HRTEM images and SAED patterns of $ZnAl_2O_4$:Tb^{3+} (3 & 5 mol %) nanophosphor synthesized with 5 h sonication time was shown in Fig. S3. TEM images shows thin sheet like nanostructures of $ZnAl_2O_4$:Tb^{3+} nanophosphor. The HRTEM image shows the well - defined crystal planes with an average spacing of ~0.28 and 0.32 nm (Fig.S3(c & d)). The SAED patterns were well matched with the (h k l) values corresponding to the prominent peaks of the PXRD profiles which is discussed in the subsequent section.

The PXRD patterns of undoped and $ZnAl_2O_4$: Tb^{3+} (0.25 - 5 mol %) nanophosphor was shown in Fig.7 (a). The obtained patterns exhibits cubic phase and were well indexed with JCPDS No. 82-1043 (Ravikumar et el., 2014b). As the concentration of dopant Tb^{3+} increases in $ZnAl_2O_4$, no appreciable shift in diffraction peaks was observed which indicate the Tb^{3+} ions were successfully occupied in the host sites. The average crystallite size (D) of the prepared samples was calculated from both W- H plots (Fig. 7 (b)) and Scherrer's relation

(Darshan et al., 2016) and the obtained values were listed in Table 1. It was evident that the value of "D" was found to decrease with increase of dopant concentration. The PXRD profile of the synthesized sample under ultrasound method exhibits more intense peak and appreciable line broadening were observed as compared to samples synthesized by using conventional stirring method (shown in blue rectangle in Fig.8). These results were evident for the smaller crystalline size of the prepared sample using ultrasound method as compared to mechanical stirring method. In addition, PXRD pattern of prepared phosphor using stirrer method exhibits the presence of traces of by-products due to incomplete reaction of solution (traces shown with star mark in Fig.8).

To investigate the various structural parameters, Rietveld refinement of $ZnAl_2O_4:Tb^{3+}$ (3 mol %) nanophosphor has been performed using *FullProf* software (Rodriguez, 2010). The Rietveld refined parameters namely occupancy, atomic functional positions of the product was listed in Table 2. It was observed that the prepared samples exhibit cubic crystal structure with lattice parameter a = 8.0707 Å, V = 525.696 $Å^3$ and space group = $Fd\bar{3}m$. The refined parameters elucidate that the $ZnAl_2O_4$ belong to the Oh_7 group with a tetrahedral coordination for the Zn^{2+} ion at 8a positions and a trigonal distorted octahedron surrounding the Al^{3+} site at 16d positions. In normal spinels all the octahedral positions were occupied by Zn^{2+} ions. If the spinel was partially inverse, some Zn^{2+} ions occupy 16d positions and some Al^{3+} ions occupy 8a positions (Ravikumar et el., 2014b). The refined XRD profile of $ZnAl_2O_4:Tb^{3+}$ (3 mol %) was shown in Fig.S4 (a). Further, refined parameter was used as inputs for the construction of packing diagram using Diamond software and was depicted in Fig.S4 (b).

Fig.S5. shows the FTIR spectra of undoped and Tb^{3+} (0.5, 1 and 3 mol %) doped $ZnAl_2O_4$ nanophosphor. The bands at ~ 3443 and 1645 cm^{-1} were attributed to –OH stretching vibrations and deformative water molecules. Further, the band at ~ 1524 cm^{-1} was

attributed to Al-O stretching vibration. The band at ~ 489, 574 and 680 cm^{-1} was due the stretching vibrations (tetrahedral and octahedral) in the host lattice (Ravikumar et el., 2014b).

Fig.9 (a) shows the TL glow curves of $ZnAl_2O_4$: Tb^{3+} (0.25 - 5 mol %) nanophosphor irradiated with 5 kGy γ - dose. A symmetric peak at 194 °C was recorded for all doped samples. It was observed that the intensity increases upto 3 mol % and then decreases. The traps of the $ZnAl_2O_4$:Tb^{3+} (3 mol %) nanophosphor acquire the maximum capacity to trap charge carriers. Further, the TL glow curves of $ZnAl_2O_4$: Tb^{3+} (3 mol %) nanophosphor synthesized with and without ultrasound irradiation under same irradiation dose (5 kGy) was shown in Fig.9 (b). It was observed that, TL intensity found to be more in ultrasound irradiation when compared to normal stirring. Fig.9 (c) depicts the TL response of the optimum $ZnAl_2O_4$: Tb^{3+} (3 mol %) nanophosphor was investigated over the different gamma dose range from 0.1 – 6 kGy at a heating rate of 2.5 °C s^{-1}. A unique with intense peak at 197 °C was observed for the entire range of samples. The integrated area of the curve (197 °C) increases up to 5 kGy gamma dose after that it diminishes (Fig.9c). This was mainly due to concentration quenching phenomena and was commonly observed for all the systems. As the dopant ion concentration increases, ions may act as self-quencher by undergone non-radiative cross transitions resulting in quenching of luminescence (Premkumar et al., 2012d). Further, it was observed that, with increase in the γ-dose, the peak positions were slightly shifted towards higher temperature side. This was due to luminescent centers/ traps as well as the site symmetry of the dopant ion in the host material [29]. Fig.9d witnessed the good linearity in the lower gamma doses (5kGy), while for higher γ-doses (>5kGy) the sample display sub-linear behavior. This linearity behavior was extremely beneficial in radiation dosimetry for the measurement of high γ-doses (Sunitha et al., 2012c).

The sub-linear behavior of TL intensity with various γ-doses can be described with the help of Track interaction model (TIM) (Horowitz et al., 1996). The luminescent centers

produced through γ- doses depend on the length and cross-section of the tracks in the $ZnAl_2O_4$ host matrix. In smaller sized particles especially in nanostructured materials, the size of the track was very much less therefore, for lower γ- irradiated samples the trap centre/ luminescent centre (TC/LC) will be fewer due to smaller sized particles which may miss during γ- exposures. On the other hand, with increase the γ exposures the particles which were missed previously will now start generating TCs/LCs resulting in increase in TL intensity. Still further increase in γ exposures, the overlapping of the defect centre (tracks) takes place due to which the production of TCs/LCs saturates causing saturation or decrease in TL intensity (Manjunatha et al., 2012).

Fig.10 shows the effect of various heating rates (2, 3 and 5 ° C s^{-1}) on TL peaks of $ZnAl_2O_4$: Tb^{3+} (3 mol %) nanophosphor on γ - irradiated (5 kGy) was studied. It was observed that with the increase in heating rate, TL peak shifted towards higher temperature side. Further, increase in heating rate, the TL intensity diminishes due to thermal quenching phenomena. This non - radiative thermal quenching phenomenon was due to discharge of charge carriers from traps and was not recombining at recombination centers and non-radiative transitions were responsible transformation of energy (Umesh et al., 2014). Fading characteristics of $ZnAl_2O_4$:Tb^{3+} (3 mol %) nanophosphor was presented as inset of Fig.10.

A phosphor which shows good dosimetric applications, the glow curve should be single a unique peak requires a finely resolved TL with simple trap distribution. A TL peaks was related to the trap levels which were present in the band gap of a solid material. These trap levels were considered by estimating diverse kinetic parameters (E, b, and s) related with these levels. The complete kinetic parameters were discussed in literature (Ravikumar et al., 2014b). The dosimetric nature of prepared samples was discussed based on its kinetic parameters. Consequently, various methods were used to estimate the kinetic parameters of

trap levels. In the present studies, four different methods were employed to estimate the kinetic parameters.

3.1. Estimation of kinetic parameters by various methods

(i) Chen's method

The activation energy 'E' was calculated by employing the Chen's set of empirical equations as discussed in the literature (Chen et al., 1981). The form factor (μ_g) was estimated and found to be in the range 0.42 - 0.47. Generally, for first and second order kinetics (μ_g) close to 0.42 and 0.52 respectively (Manjunatha et al., 2012). Therefore, in the present case order of kinetics was found to be unity. The frequency factor (s) was estimated by using following equation;

$$s = \frac{\beta E}{kT_m^2}\exp\left(\frac{E}{kT_m}\right)\left[1+(b-1)\Delta_m\right]^{-1} \qquad \text{---------- (12)}$$

where, $\beta = \frac{dT}{dt}$, $\Delta_m = \frac{2kT_m}{E}$ and $\Delta = \frac{2kT}{E}$

(ii) Grosweiner method

The 'E' and 's' values estimated using as per literature (Hari Krishna et al., 2014). The values were calculated and summarized in Table 3.

(iii) Luschiks method

The 'E' and 's' values estimated using the relation (Premkumar et al., 2012e);

$$E = 0.978\frac{kT_m^2}{\delta} \qquad \text{---------- (13)}$$

$$s = 0.976\left(\frac{\beta}{\delta}\right)\exp\left(0.976\frac{T_m}{\delta}\right) \qquad \text{---------- (14)}$$

where $\delta = T_2 - T_m$, β; the heating rate, T_m; maximum temperature peak

The values of 'E' and 's' of $ZnAl_2O_4$: Tb^{3+} (3 mol %) nanophosphor was estimated from above methods and listed in Table 3. Further, fading characteristics of prepared optimum $ZnAl_2O_4$: Tb^{3+} (3 mol %) nanophosphor was monitored at RT. The observed fading was ~25 % over a period of 30 days. The obtained value is high enough to be considered as significant TLD phosphor in dosimetry.

Fig. 11 shows the PL excitation spectrum of $ZnAl_2O_4$: Tb^{3+} (0.25-5 mol %) nanophosphor monitored at 543 nm emission. The spectra exhibit a series of peaks at ~ 317, 350 and 379 nm corresponds to 4f–4f transitions of dopant Tb^{3+} ions (Darshan et al., 2016c). Fig.12(a) depicts the PL emission spectra of $ZnAl_2O_4$:Tb^{3+} (0.25- 5 mol %) nanophosphor excited at 379 nm at RT. The spectra consist of characteristic peaks at ~ 489, 543, 586 and 621 nm due to $^5D_4 \rightarrow {}^7F_6$, $^5D_4 \rightarrow {}^7F_5$, $^5D_4 \rightarrow {}^7F_4$ and $^5D_4 \rightarrow {}^7F_3$ transitions respectively (Darshan et al., 2016c).The peaks at ~ 543 nm (green emission) and 489 nm (blue emission) were due to magnetic dipole (MD) transition and electric dipole (ED) transitions of Tb^{3+} ions respectively (Darshan et al., 2016c). The PL spectra of $ZnAl_2O_4$: Tb^{3+} (3 mol %) nanophosphor with and without ultrasound was shown in Fig.12 (b). Figure clearly shows that both the curves exhibit similar behavior but difference in PL intensity. Further, asymmetry ratio (A_{21}) was used to determine the degree of distortion from the inversion symmetry of the local environment of the Tb^{3+} ions in host matrix with varying Tb^{3+} concentration (Venkatachalaiah et al., 2017a).

$$A_{21} = \frac{\int I_2\left({}^5\mathrm{D}_4 \rightarrow {}^7\mathrm{F}_6\right)d\lambda}{\int I_1\left({}^5D_4 \rightarrow {}^7F_5\right)d\lambda} \qquad \text{--------- (15)}$$

where I_1 and I_2; intensities of MD and ED transition respectively. The variation of A_{21} with varying Tb^{3+} concentration in $ZnAl_2O_4$: Tb^{3+} (0.25-5 mol %) nanophosphor was listed in Table.4. Fig.12(c) depicts the effect of various Tb^{3+} concentrations on PL emission intensity in the $ZnAl_2O_4$ host. It was observed that, the PL intensity was increased upto 3 mol % of

Tb^{3+} concentration and afterwards decreases. The diminution of PL intensity was due to concentration quenching phenomena resulting from energy transfer between Tb^{3+} ions.

To know the type of interaction involved in energy transfer phenomena can be estimated using Van Uitert theory (Van Uitert, 1971). The emission intensity (I) per activator ion given in following equation;

$$\frac{I}{X} = K\left(1+\beta(X)^{Q/3}\right)^{-1} \quad \text{---------- (16)}$$

where X ; Tb^{3+} ion concentration, K and β; constants for a given excitation (λ = 379 nm) and Q; a constant of multi- polar interaction (dipole – dipole (d–d); dipole – quadrupole (d– q) and quadrupole – quadrupole (q–q) interactions when Q is equal to 6, 8 and 10 respectively)

$$Log\frac{I}{\chi} = A - \frac{Q}{3}\log\chi \quad \text{---------- (17)}$$

where $\left(A = \log k - \log\beta\right)$. Fig.12 (d) shows the curve of log I/χ v/s. log χ for $ZnAl_2O_4$:Tb^{3+} (0.25-5 mol %) nanophosphor and which clears that the relation was approximately linear and the slope of the line was ~ -1.926. The calculated value Q was found to be 6.64 was almost equal 6. This value shows that concentration quenching phenomena in $ZnAl_2O_4$: Tb^{3+} nanophosphor was due to d-d transition.

The J-O intensity parameters (Ω_2 & Ω_4), radiative transition probability, lifetime, branching and asymmetric ratio were evaluated and tabulated in Table 4. The intensity of the hyper sensitive electric dipole ($^5D_4 \rightarrow {}^7F_5$) transition depends on the local symmetry of the Tb^{3+} ions in the host. The value Ω_2 was due to structural changes or covalency of Tb^{3+} ions and also depends on short range effects. The change in values of Ω_2 observed in Table 4 was attributed to distortions present around the dopant Tb^{3+} ion sites. As the concentration of Tb^{3+}

ions increases, the value of Ω_2 was also increases which show that high covalence of the metal–ligand bonds of Tb^{3+} ion sites in the host matrix. The parameter Ω_4 was due to the long range effects and symmetry of the Tb^{3+} ion. Its value increases with increase in the dopant Tb^{3+} concentration, results the decrease in the electron density on the ligands. The measured branching ratio of $ZnAl_2O_4$: Tb^{3+} nanophosphor were found to be ~ 0.9 > 0.50. Therefore, the present phosphor was suitable for green color emitting display devices.

Fig.13 (a) shows the CIE (International Commission on Illumination) (Darshan et al., 2016d; Venkatachalaiah et al., 2017b) chromaticity diagram of the prepared $ZnAl_2O_4$: Tb^{3+} (0.25 - 5 mol %) nanophosphor. CIE color co-ordinates (x, y) were calculated and listed in Table 5. CIE co-ordinates for the prepared samples were located in 'green' region. Further, the correlated color temperature (CCT) was assessed by Planckian locus, which was only a small portion of the (x, y) chromaticity diagram and there exist many operating points outside the Planckian locus (Basavaraj et al., 2017). The CCT diagram of $ZnAl_2O_4$: Tb^{3+} (0.25-5 mol %) nanophosphor was shown in Fig. 13 (b) and the obtained values were summarized in Table 5. Based on the obtained results, it was clear that the present phosphor is found to be highly useful in solid-state lighting and display devices fabricated with UV (InGaN) or blue (GaN) chips.

4. Conclusions

A series of $ZnAl_2O_4$: Tb^{3+} (0.25 - 5 mol %) nanophosphor were synthesized by self–sacrificial *A.V.* gel assisted ultrasonication method. The typical ultrasound synthesis method offered more advantages including fast and simple process with exceptional reproducibility. The various structural evolutions of present samples were systematically investigated by SEM studies. Gamma induced TL studies in the range 100 Gy to 1 kGy exhibit a well resolved glow with peak at 197 °C. The intensity at the glow peak temperature increase

linearly up to 5 kGy and then it decrease with further increase of γ- dose. Up to 5 kGy the phosphor was quite useful for TL dosimetry. The PL spectra evidence that present phosphor emits bright green color under near ultra violet excitation (379 nm). The photometric characteristics of the synthesized phosphors were estimated by using PL data. The present work explores new possibilities to the design of new engineered nanostructures for display devices and dosimetry materials.

References

Amith Yadav, H. J., Eraiah, B., Nagabhushana, H., Darshan, G. P., Daruka Prasad, B., Sharma, S.C., Premkumar, H. B., Anantharaju, K. S., Vijayakumar, G. R., 2017. Facile ultrasound route to prepare micro/nano superstructures for multifunctional applications. ACS Sustainable Chem. Eng. *5* (3), 2061–2074.

Basavaraj, R.B., Nagabhushana, H., Darshan, G.P., Daruka Prasad, B., Sharma, S.C., Venkatachalaiah, K.N., 2017. Ultrasound assisted rare earth doped Wollastonite nanopowders: Labeling agent for imaging eccrine latent fingerprints and cheiloscopy applications. J. Ind. Eng. Chem. 51, 90-105.

Basavaraj , R. B., Nagabhushana, H., Daruka Prasad, B., G. R. Vijaya Kumar, 2017, Zinc silicates with tunable morphology by surfactant assisted sonochemical route suitable for NUV excitable white light emitting diodes, Ultrasonics Sonochemistry, 34, 700-712.

Burda, C., Chen, X., Narayanan, R., El-Sayed, M. A., 2005. Chemistry and properties of nanocrystals of different shapes. Chem. Rev.105, 1025-1102.

Boudreau, M.D., Beland, F.A., 2006. An evaluation of the biological and toxicological properties of *Aloe barbadensis* (Miller) A.V. J. Environ. Sci. Health Part C 24, 103-154.

Cheng, B., Qu, S., Zhou, H., Wang, Z., 2006. Porous $ZnAl_2O_4$ spinel nanorods doped with Eu^{3+}: synthesis and photoluminescence. Nanotech. 17, 2982-2987.

Chandran, S.P., Chaudhary, M., Pasricha, R., Ahmad, A., Sastry, M., 2006. Synthesis of gold nanotriangles and silver nanoparticles using *A.V.* plant extract. Biotechnol. Prog. 22, 577-583.

Chen, R., Kirish, Y., 1981. Analysis of Thermally Stimulated Processes, Pergamon, NewYork.

Ciupina, V., Carazeanu, I., Prodan, G., 2004. Characterization of $ZnAl_2O_4$ nanocrystals prepared by co precipitation and micro emulsion techniques. J. Optoelect. Adv. Mater. 6, 1317-1322.

Dimitrijevic, N. M., Saponjic, Z. V., Rabatic, B. M., Poluektov, O. G., Rajh, T., 2007. Effect of size and shape of nanocrystalline TiO_2 on photogenerated charges, An EPR study. J. Phys. Chem. C, 111, 14597-14601.

Darshan, G.P., Premkumar, H.B., Nagabhushana, H., Sharma, S.C., Prashantha, S.C., Daruka Prasad,B.,2016. Effective fingerprint recognition technique using doped yttrium aluminate nanophosphor material. J. Colloid Interface Sci. 464, 206-218.

Darshan, G.P., Premkumar, H.B., Nagabhushana, H., Sharma, S.C., Prashantha, S.C., Nagaswarupa, H.P., Daruka Prasad, B., 2016. Blue light emitting ceramic nano-pigments of Tm^{3+} doped $YAlO_3$: Applications in latent finger print, anti-counterfeiting and porcelain stoneware. Dyes Pigm. 131, 268-281.

Darshan, G.P., Premkumar, H.B., Nagabhushana, H., Sharma, S.C., Daruka Prasad, B., Prashantha, S.C., Basavaraj, R.B., 2016. Superstructures of doped yttrium aluminates for luminescent and advanced forensic investigations. J. Alloys Compd. 686, 577-587.

Darshan, G.P., Premkumar, H.B., Nagabhushana, H., Sharma, S.C., Daruka Prasad, B., Prashantha, S.C., 2016. Neodymium doped yttrium aluminate synthesis and optical properties–A blue light emitting nanophosphor and its use in advanced forensic analysis. Dyes Pigm. 134, 227-233.

Dhanalakshmi, M., Nagabhushana, H., Darshan, G.P., Basavaraj, R.B., Daruka Prasad, B., 2017. Sonochemically assisted hollow/solid $BaTiO_3$: Dy^{3+} microspheres and their applications in effective detection of latent fingerprints and lips prints. J. Sci.: Adv. Mater. Devices 2, 22-33.

Ekaterina V. Skorb, Daria V. Andreevac, 2013. Bio-inspired ultrasound assisted construction of synthetic sponges. J. Mater. Chem. A 1, 7547.

Geeta Rani, 2017. Annealing effect on the structural, optical and thermoluminescent properties of $ZnAl_2O_4$:Cr^{3+}. Powder Tech. 312, 354–359.

Hari Krishna, R., Nagabhushana, B.M., Nagabhushana, H., Chakradhar, R.P.S., Sivaramakrishna, R., Shivakumara, C., Tiju Thomas, 2014. Auto-ignition based synthesis of Y_2O_3 for photo- and thermo - luminescent applications. J. Alloys Comp. 585, 129–137.

Hari Krishna, R., Nagabhushana, B.M., Nagabhushana, H., Monika, D.L., Sivaramakrishna, R., Shivakumara, C., Chakradhar, R.P.S., Tiju Thomas, 2014. Photoluminescence, thermoluminescence and EPR studies of solvothermally derived Ni^{2+} doped Y $(OH)_3$ and Y_2O_3 multi-particle-chain microrods. J. Lumin. 155, 125–134.

Horowitz, Y.S., Rosenkrantz, M., Mahajna, S., Yossian, D., 1996. The track interaction model for alpha particle induced thermoluminescence supralinearity: dependence of the supralinearity on the vector properties of the alpha particle radiation field. J. Phys. D: Appl. Phys. 29, 205–217.

Jin Ho Bang, Kenneth S. Suslick, 2010. Applications of Ultrasound to the Synthesis of Nanostructured Materials, Adv. Mater. 22, 1039–1059.

Judd, B. R., 1962. Optical absorption intensities of rare-earth ions. Phys Rev. 127, 750-761.

D. Kavyashree, C. J. Shilpa, H. Nagabhushana, B. Daruka Prasad, G. L. Sreelatha, S. C. Sharma, S. Ashoka, R. Anandakumari, H. B. Premkumar, 2015, ZnO Superstructures as an Antifungal for Effective Control of Malassezia furfur, Dermatologically Prevalent Yeast: Prepared by Aloe Vera Assisted Combustion Method, *ACS Sustainable Chem. Eng.*, 3, 1066–1080.

Kitis, G., Papadopoulos, G.J., Charalambous, S., Tuyn, J.W.N., 1994. The influence of heating rate on the response and trapping parameters of α-Al_2O_3:C. Radiat. Prot. Dos. 55, 183-190.

Kortov, V.S., Milman, I., Kirpa, V.I., Lesz, J., 1994. Some features of α Al_2O_3 dosimetric thermoluminescence crystals. Radiat. Prot. Dosim. 55, 279-283.

Klinkaewnarong, J., Swatsitang, E., Masingboon, C., Seraphin, S., Maensiri, S., 2010. Synthesis and characterization of nanocrystalline HAp powders prepared by using *A.V.* plant extracted solution. Curr. Appl. Phys. 10, 521-525.

Lakshmesha T R, M. K. Sateesh., B. Daruka Prasad, S. C. Sharma, D. Kavyashree, M. Chandrashekhar, H. Nagabhushana, 2014, Reactivity of Crystalline ZnO Superstructures against Fungi and Bacterial Pathogens: Synthesized Using Nerium oleander Leaf Extract, *Cryst. Growth Des.*, 14 , 4068–4079.

Laokul, P., Maensiri, S., 2009. A.V. solution synthesis and magnetic properties. J. Optoelect. Adv. Mater. 11, 857-862.

Laokul, P., Amornkitbamrung, V., Seraphin, S., Maensiri, S., 2011. Characterization and magnetic properties of nanocrystalline $CuFe_2O_4$, $NiFe_2O_4$, $ZnFe_2O_4$ powders prepared by the *A.V.* extract solution. Curr. Appl. Phys. 11, 101-108.

Lou, Z., Hao, J., 2004. Cathodoluminescence of rare-earth-doped zinc aluminate films. Thin Solid Films, 450, 334–340.

Mithlesh Kumar, Santosh K. Gupta, 2015. An insight into optical spectroscopy of intense green emitting $ZnAl_2O_4$:Tb^{3+} nanoparticles: photo, thermally stimulated luminescence and EPR study. J. Lumin. 168, 151–157.

Maensiri, S., Laokul, P., Klinkaewnarong, J., Phokha, S., Promarak, V., Seraphin, S., 2008. Indium oxide (In_2O_3) nanoparticles using *A.V.* plant extract: Synthesis and optical properties. J. Optoelectron. Adv. Mater. 10, 161-165.

Manjunatha, C., Sunitha, D.V., Nagabhushana, H., Nagabhushana, B.M., Sharma, S.C., Chakradhar, R.P.S., 2012. Combustion synthesis, structural characterization, thermo and photoluminescence studies of $CdSiO_3$:Dy^{3+} nanophosphor. Spectrochim. Acta Part A: Mole. Biomole. Spect. 93, 140–148.

Ofelt, G. S., 1962. Intensities of crystal spectra of rare-earth ions. J. Chem. Phys. 37, 511-520.

Premkumar, H.B., Ravikumar, B.S., Sunitha, D.V., Nagabhushana, H., Sharma, S.C., Savitha, M.B., Mohandas Bhat, S., Nagabhushana, B.M., Chakradhar, R.P.S., 2013. Investigation of structural and luminescence properties of Ho^{3+} doped $YAlO_3$ nanophosphors synthesized through solution combustion route. Spectrochim. Acta Part A: Mole. Biomole. Spect. 115, 234-243.

Premkumar, H.B., Nagabhushana, H., Sharma, S.C., Prashantha, S.C., Nagaswarupa, H.P., Nagabhushana, B.M., Chakradhar, R.P.S., 2014. Structural, photo and thermoluminescence studies of Eu^{3+} doped orthorhombic $YAlO_3$ nanophosphors. J. Alloys Comp. 601, 75–84.

Premkumar, H.B., Sunitha, D.V., Nagabhushana, H., Sharma, S.C., Nagabhushana, B.M., Shivakumara, C., Rao, J.L., Chakradhar, R.P.S., 2013. Synthesis, characterization, EPR, photo and thermoluminescence properties of $YAlO_3$:Ni^{2+} nanophosphors. J. Lumin. 135, 105–112.

Premkumar, H.B., Sunitha, D.V., Nagabhushana, H., Sharma, S.C., Nagabhushana, B.M., Shivakumara, C., Rao, J.L., Chakradhar, R.P.S., 2012. Thermoluminescence, photoluminescence and EPR studies on Mn^{2+} activated yttrium aluminate ($YAlO_3$) perovskite. J. Lumin. 132, 2409–2415.

Premkumar, H.B., Sunitha, D.V., Nagabhushana, H., Sharma, S.C., Nagabhushana, B.M., Rao, J.L., Kinshuk Gupta, Chakradhar, R.P.S., 2012. $YAlO_3$:Cr^{3+} nanophosphor: Synthesis, photoluminescence, EPR, dosimetric studies. Spectrochim. Acta Part A: Mole. Biomole. Spect. 96, 154–162.

Pushpa Kumari, Dwivedi, Y., 2016. Structural and photophysical investigations of bright yellow emitting Dy: $ZnAl_2O_4$ nanophosphor. J. Lumin. 178, 407–413.

Phumying, S., Labuayai, S., Swatsitang, E., Amornkitbamrung, V., Maensiri, S., 2013. Nanocrystalline spinel ferrite (MFe_2O_4, M = Ni, Co, Mn, Mg, Zn) powders prepared by a simple *A.V.* plant-extracted solution hydrothermal route. Mater. Res. Bull. 48, 2060-2065.

Patel, V.K., Bhattacharya, S., 2013. High-performance nanothermite composites based on aloe-vera directed CuO nanorods. ACS Appl. Mater. Interfaces 5, 13364–13374.

Rui Yang, Aijun Han, Mingquan Ye, Xingxing Chen, Lin Yuan, 2017. The influence of Mn/N-codoping on the thermal performance of $ZnAl_2O_4$ as high near-infrared reflective inorganic pigment. J. Alloys Comp. 696, 1329–1341.

Rusu, E., Ursaki, V., Novitschi, G., Vasile, M., Petrenco, P., Kulyuk, L., 2009. Luminescence properties of $ZnGa_2O_4$ and. $ZnAl_2O_4$ spinels doped with Eu^{3+} and Tb^{3+} ions. Phys. Status Solidi. C 6, 1199-1202.

Reynolds, T., Dweck, A.C., 1999. A.V. leaf gel: a review update. J. Ethnopharmacol. 68, 3-37.

Ravikumar, B.S., Nagabhushana, H., Sharma, S.C., Nagabhushana, B.M., 2014. Low temperature synthesis, structural and dosimetric characterization of $ZnAl_2O_4:Ce^{3+}$ nanophosphor. Spectrochim. Acta Part A: Mole. Biomole. Spect. 122, 489–498.

Ravikumar, B.S., Nagabhushana, H., Sunitha, D.V., Sharma, S.C., Nagabhushana, B.M., Shivakumara, C., 2014. Plant latex mediated green synthesis of $ZnAl_2O_4:Dy^{3+}$ (1–9 mol %) nanophosphor for white light generation. J. Alloys Comp. 585, 561-571.

Rodriguez-Carvajal, J., 2010. Full Comput. Program.

Sunitha, D.V., Nagabhushana, H., Sharma, S.C., Nagabhushana, B.M., Daruka Prasad, B., Chakradhar, R.P.S., 2014. Study on low temperature solution combustion synthesized $Sr_2SiO_4:Dy^{3+}$ nano phosphor for white LED. Spectrochim. Acta Part A: Mole. Biomole. Spect. 127, 381–387.

Sunitha, D.V., Nagabhushana, H., Sharma, S. C., Fouran Singh, Nagabhushana, B. M., Dhananjaya, N., Shivakumara, C., Chakradhar, R.P.S., 2013. Structural, iono and thermoluminescence properties of heavy ion (100 MeV Si^{7+}) bombarded $Zn_2SiO_4:Sm^{3+}$ nanophosphor. J, Lumin.143, 409–417.

Sunitha, D.V., Manjunatha, C., Shilpa, C.J., Nagabhushana, H., Sharma, S.C., Nagabhushana, B.M., Dhananjaya, N., Shivakumara, C., Chakradhar, R.P.S., 2012. $CdSiO_3$: Pr^{3+} nanophosphor: Synthesis, characterization and thermoluminescence studies. Spectrochim. Acta Part A: Mole. Biomole. Spect. 99, 279–287.

Shivaram, M., Hari Krishna, R., Nagabhushana, H., Sharma, S.C., Nagabhushana, B.M., Ravikumar, B.S., Dhananjaya, N., Shivakumara, C., Rao, J.L., Chakradhar, R.P.S., 2013. Synthesis, characterization, EPR and thermoluminescence properties of $CaTiO_3$ nanophosphor. Mater. Res. Bull. 48, 1490–1498.

Strek, W., Deren, P., Bednarkiewicz, A., Zawadzki, M., Wrzyszcz, J., 2000. Emission properties of nanostructured Eu^{3+} doped zinc aluminate spinels. J. Alloys Comp. 300, 456–458.

Suresh, C. Nagabhushana, H., Darshan, G.P., Basavaraj, R.B., Daruka Prasad, B., Sharma, S.C., Sateesh, M.K., Shabaaz Begum, J.P., 2017. Lanthanum oxyfluoride nanostructures prepared by modified sonochemical method and their use in the fields of optoelectronics and biotechnology. Arabian J. Chem. doi.org/10.1016/j.arabjc.2017.03.006.

Sankar, R., Manikandan, P., Malarvizhi, V., Fathima, T., Shivashangari, K.S., Ravikumar, V., 2014. Green synthesis of colloidal copper oxide nanoparticles using *Carica papaya* and its application in photocatalytic dye degradation. Spectrochim. Acta Part A: Mole. Biomole. Spect. 121, 746-750.

Shin, K.H., Woo, W.S., Lim, S.S., Shim, C.S., Chung, H.S., Kennely, E.J., Kinghorn, A.D., 1997. Elgonica-dimers A and B, two potent alcohol metabolism inhibitory constituents of *Aloe arborescens*. J. Nat. Prod. 60, 1180-1182.

Saccu, D., Bagoni, P., Procida, G.J., 2001. Aloe exudate: Characteriza- tion by reversed phase HPLC and headspace GC-MS. J. Agric. Food Chem. 49, 4526-4530.

Som, S., Kunti, A. K., Kumar, V., Kumar, V., Dutta, S., Chowdhury, M., Sharma, S. K., Terblans, J. J., Swart, H. C., 2014. Defect correlated fluorescent quenching and electron phonon coupling in the spectral transition of Eu^{3+} in $CaTiO_3$ for red emission in display application. J. Appl. Phys.115, 193101–193114.

Som, S., Choubey, A., Sharma, S. K., 2012. Luminescence studies of rare earth doped yttrium gadolinium mixed oxide phosphor. Physica B 407, 3515-3519.

Suslick, K. S., Doktycz, S. J., 1990. Advances in Sonochemistry. JAI Press, New York 1, 197.

Thinesh Kumar, R., Clament Sagaya Selvam, N., Ragupathi, C., John Kennedy, L., Judith Vijaya, J., 2012. Synthesis, characterization and performance of porous Sr (II) - added $ZnAl_2O_4$ nanomaterials for optical and catalytic applications. Powder Techn. 224, 147-154.

Umano, K., Nakahara, K., Shoji, A., Shibamoto, T., 1999. Aroma chemicals isolated and identified from leaves of Aloe arborescens Mill. Var. Natalensis Berger. J. Agric. Food Chem. 47, 3702-3705.

Umesh, B., Nagabhushana, H., Sharma, S.C., Eraiah, B., Dhananjaya, N., Nagabhushana, B.M., Rao, J.L., Chakradhar, R.P.S., 2014. Nd_2O_3:Gd^{3+} nanocrystalline phosphor: γ-Induced thermoluminescence, EPR and structural properties. J. Alloys and Comp. 591, 286–292.

Vossmeyer, T., Katsikas, L., Giersig, M., Popovic, I. G., Diesner, K., Chemseddine, A., Eychmuller, A., Weller, H., 1994. CdS Nanoclusters: Synthesis, characterization, size dependent oscillator strength, temperature shift of the excitonic transition energy, and reversible absorbance shift. J. Phys. Chem. 98, 7665-7673.

Visinescu, D., Jurca, B., Ianculescu, A., Carp, O., 2011. Starch – A suitable fuel in new low-temperature combustion-based synthesis of zinc aluminate oxides. Polyhedron 30, 2824-2831.

Varma, R.S., 2012. Greener approach to nanomaterials and their sustainable applications. Chem. Eng. 1, 123-128.

Van der Laag, N.J., Snel, M.D., Magusin, P.C.M.M., de With, G., 2004. Structural, elastic, thermophysical and dielectric properties of zinc aluminate ($ZnAl_2O_4$). J. Euro. Ceram. Soc. 24, 2417-2424.

Venkataravanappa, M., Nagabhushana, H., Daruka Prasad, B., Darshan, G.P., Basavaraj, R.B., Vijayakumar, G.R., 2017. Dual color emitting Eu doped strontium orthosilicate phosphors synthesized by bio-template assisted ultrasound for solid state lightning and display applications. Ultrason. Sonochem. 34, 803–820.

Venkataravanappa, M., Nagabhushana, H., Darshan, G.P., Daruka Prasad, B., Vijayakumar, G.R., Premkumar, H.B. Udayabhanu, 2016. Novel EGCG assisted ultrasound synthesis of self-assembled Ca_2SiO_4: Eu^{3+} hierarchical superstructures: Photometric characteristics and LED applications. Ultrason. Sonochem. 33, 226–239.

Van Uitert, L., 1971.Energy transfer between rare earth ions in tungstates. J. Lumin. 4, 1.

Venkatachalaiah, K.N., Nagabhushana, H., Darshan, G.P., Basavaraj, R.B., Daruka Prasad, B., 2017. Novel and highly efficient red luminescent sensor based$SiO_2@Y_2O_3$:Eu^{3+}, M^+(M^+= Li, Na, K) composite core–shell fluorescent markers for latent fingerprint recognition, security ink and solid state lightning applications. Sens. Actu. B 251, 310–325.

Venkatachalaiah, K.N., Nagabhushana, H., Darshan, G.P., Basavaraj, R.B., Daruka Prasad, B., Sharma, S. C., 2017. Blue light emitting Y_2O_3:Tm^{3+} nanophosphors with tunable morphology obtained by bio-surfactant assisted sonochemical route. Spectrochim. Acta Part A: Mole. Biomol. Spect. 184, 89–100.

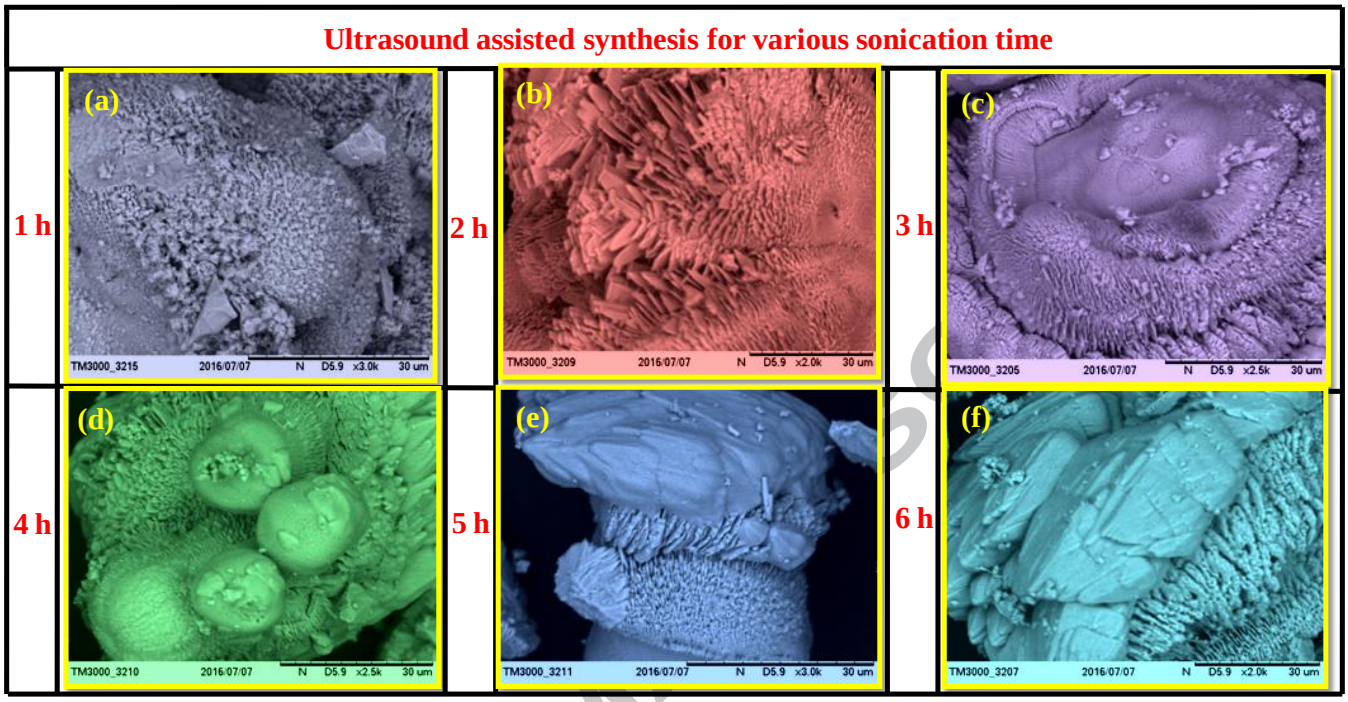

Fig.1. SEM images of $ZnAl_2O_4$: Tb^{3+} (3 mol %) nanophosphor synthesized with different sonication time (1, 2, 3, 4, 5 and 6 h) with 20 ml *A.V.* gel concentration.

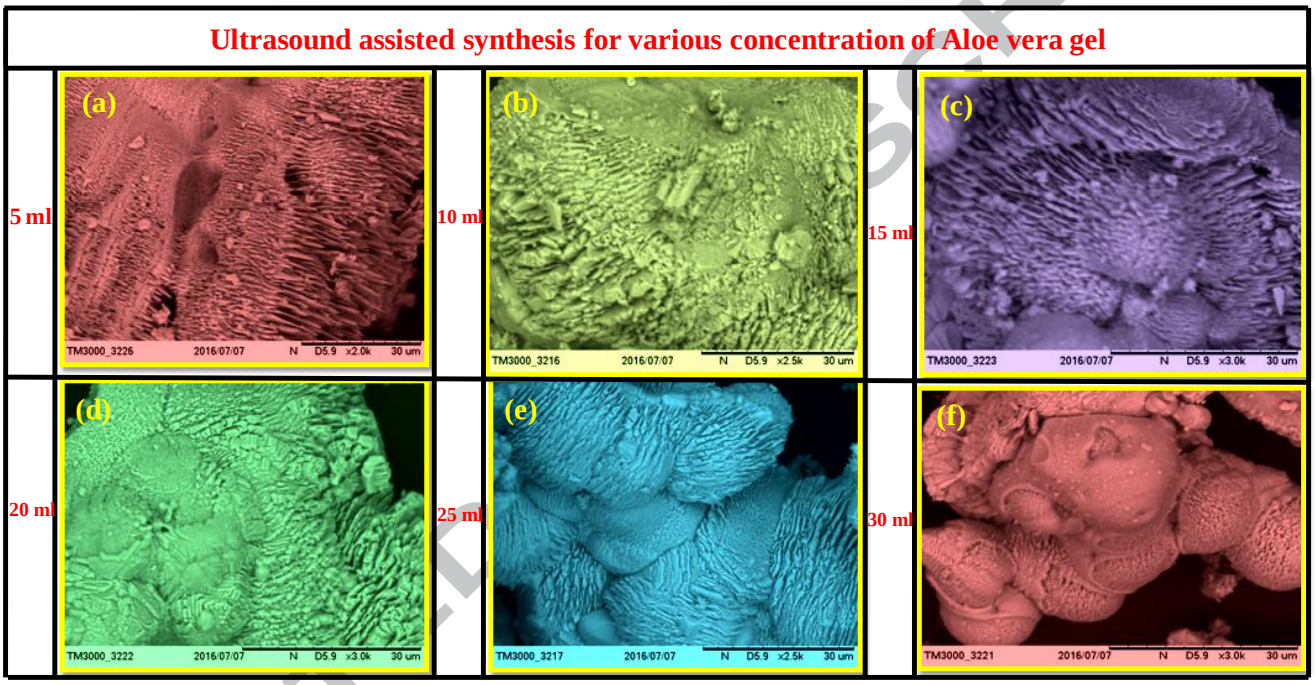

Fig.2. SEM images of $ZnAl_2O_4$: Tb^{3+} (3 mol %) nanophosphor fabricated with different concentration of *A.V.* gel (5, 10, 15, 20, 25 and 30 ml) with 5 h of ultrasonic irradiation time.

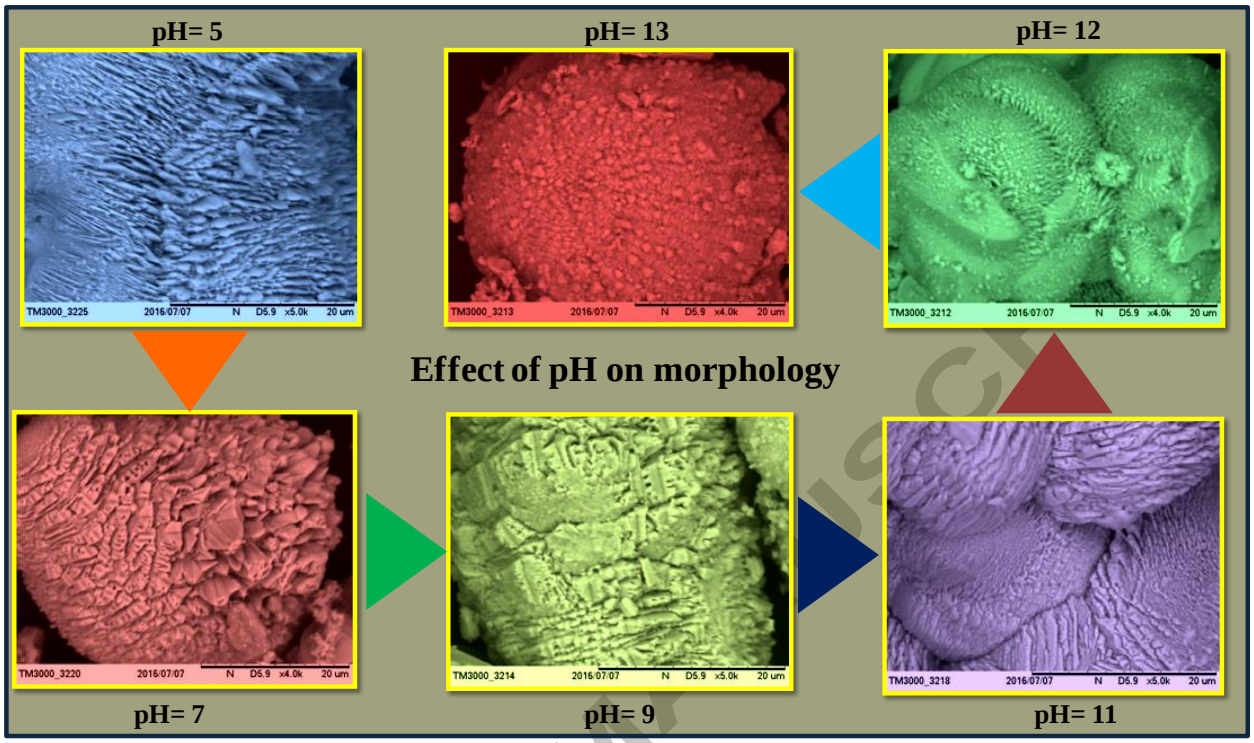

Fig.3.SEM images of $ZnAl_2O_4$: Tb^{3+} (3 mol %) nanophosphor synthesized with various pH values (5, 7, 9, 11, 12 and 13) with 5 h of ultrasonic irradiation time and 25 ml of *A.V.* gel.

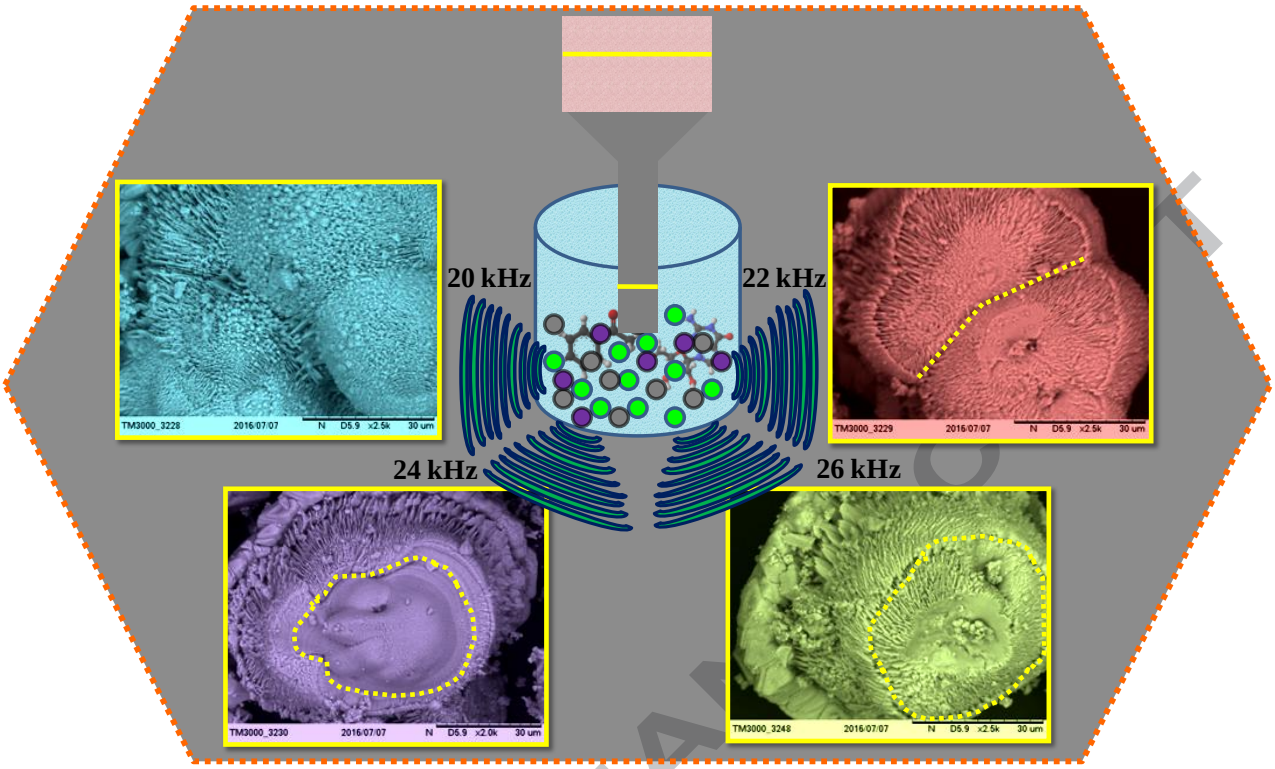

Fig.4. SEM images of $ZnAl_2O_4$: Tb^{3+} (3 mol %) nanophosphor synthesized with different sonication power (20, 22, 24 and 26 kHz) with 5 h of ultrasonic irradiation time and 25 ml of *A.V.* gel.

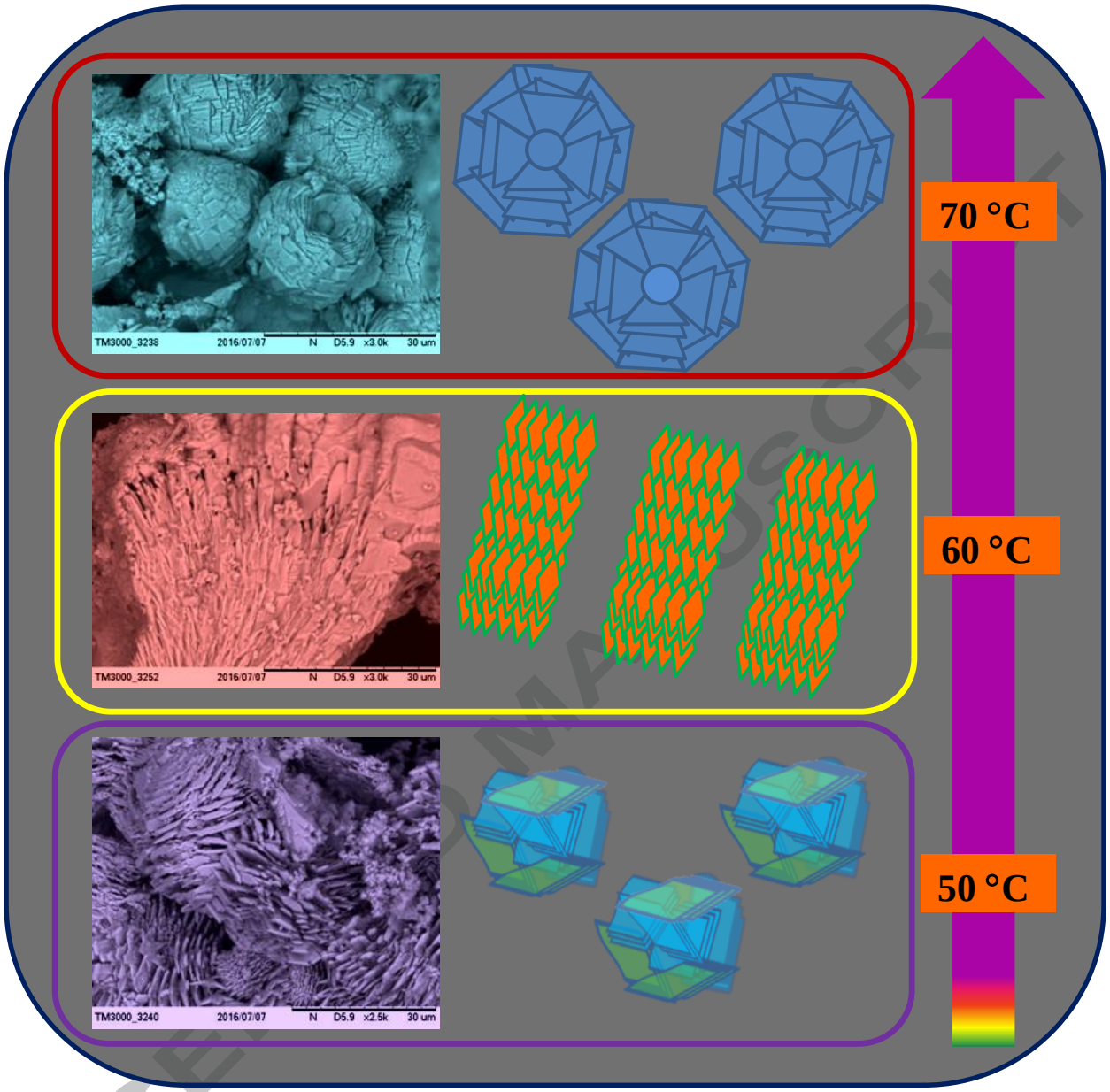

Fig.5. SEM images of $ZnAl_2O_4$: Tb^{3+} (3 mol %) nanophosphor prepared with different temperature (50, 60 and 70 °C) with 5 h of ultrasonic irradiation time.

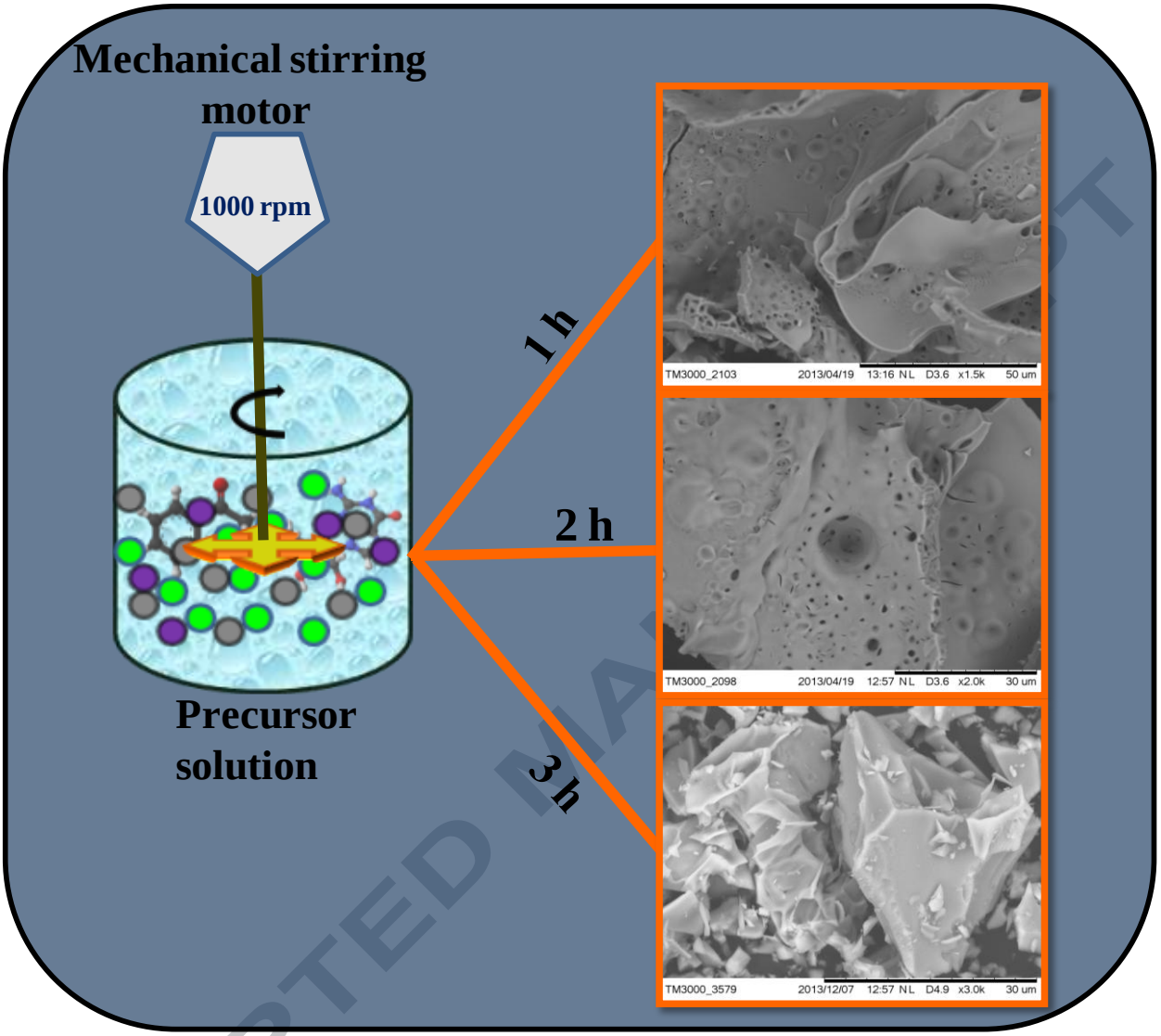

Fig.6. SEM images of $ZnAl_2O_4$: Tb^{3+} (3mol %) nanophosphor obtained with mechanical stirring by different time (1, 2, and 3 h,) with 30 ml of *A.V.* gel.

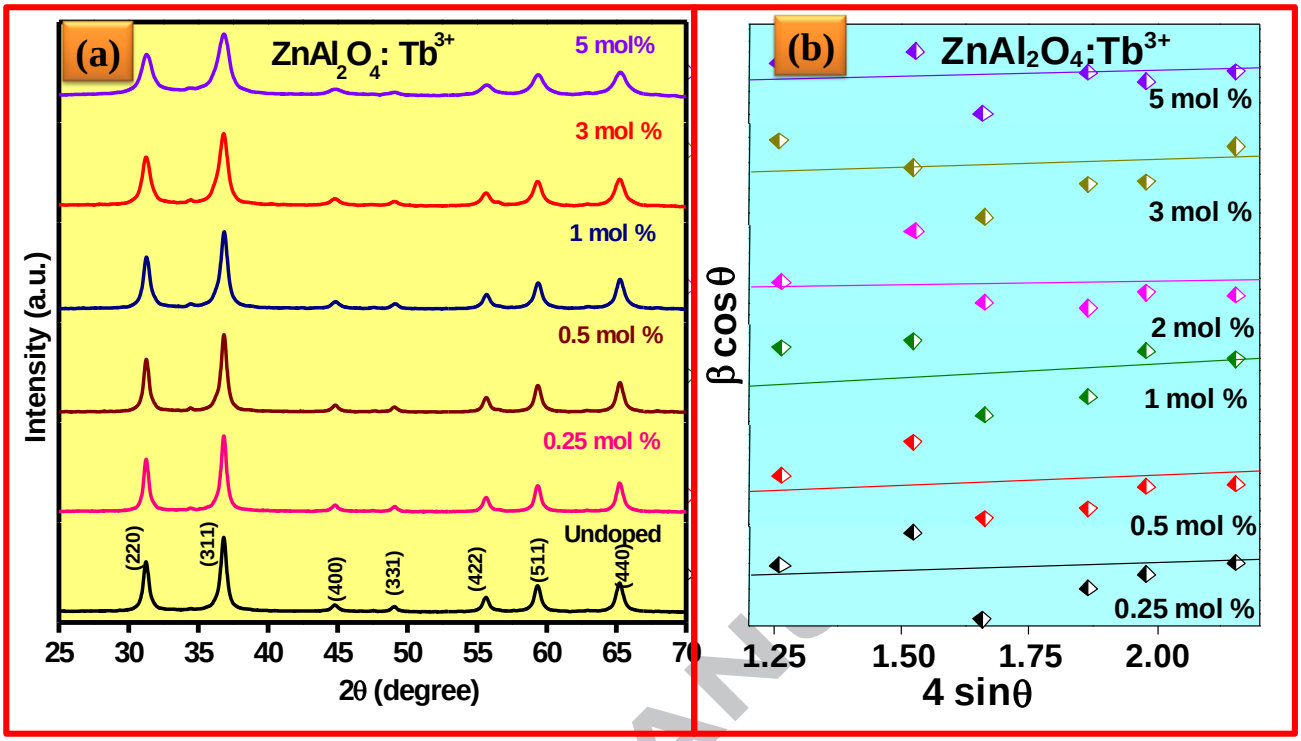

Fig.7. PXRD patterns and (b) W–H plots of $ZnAl_2O_4$: Tb^{3+} (0.25 - 5 mol %) nanophosphor.

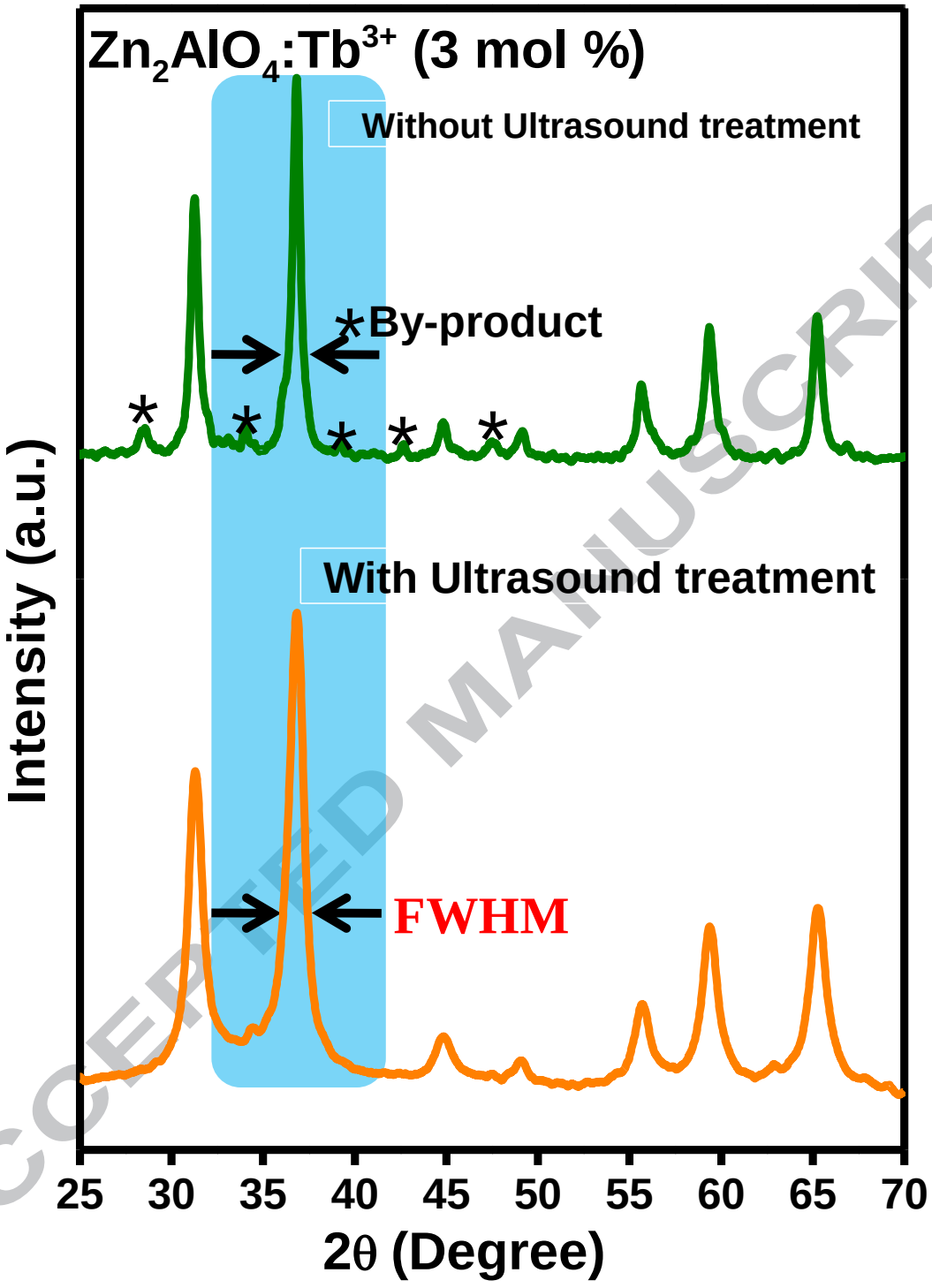

Fig.8. PXRD patterns of $ZnAl_2O_4$: Tb^{3+} (3 mol %) nanophosphor synthesized with and without ultrasonic irradiation.

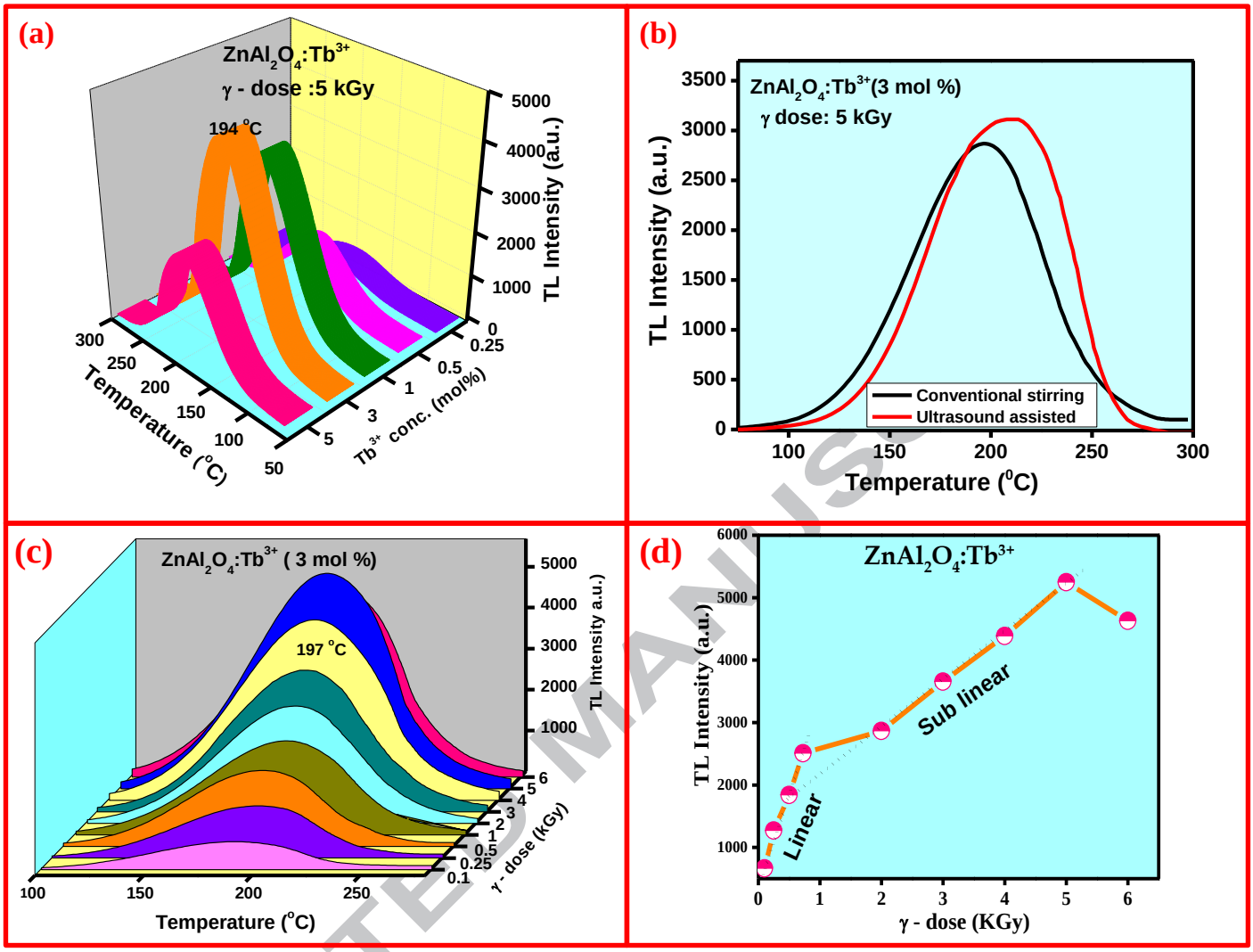

Fig. 9(a) TL glow curves of $ZnAl_2O_4$: Tb^{3+} (0.25 – 5 mol %) nanophosphor irradiated with 5 kGy γ - dose, (b) TL glow curves of $ZnAl_2O_4$: Tb^{3+} (3 mol %) nanophosphor with and without ultrasound irradiation, (c) TL glow curves of $ZnAl_2O_4$: Tb^{3+} (3 mol %) nanophosphor irradiated to different γ - dose and (d) Variation of TL glow peak intensity at 197 °C with different γ - doses (0.1 – 6 k Gy).

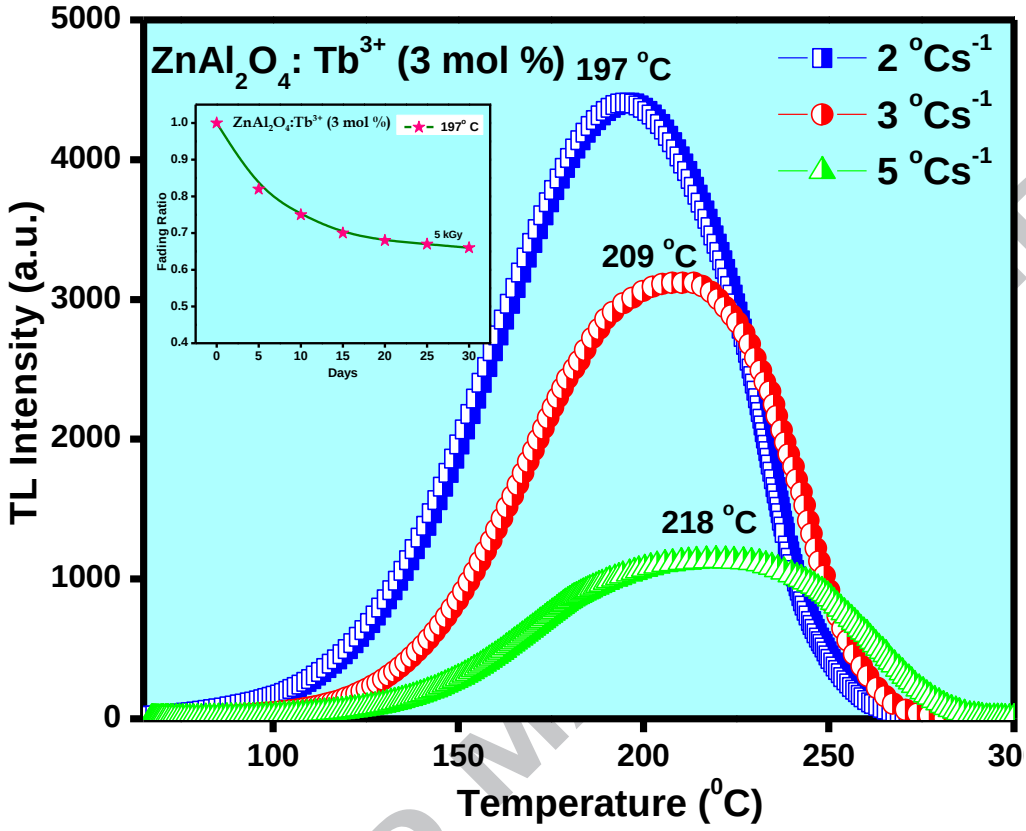

Fig.10. TL glow curves of $ZnAl_2O_4$: Tb^{3+} (3 mol %) nanophosphor recorded for different heating rates (γ dose = 5 kGy) [Inset: Fading characteristics of $ZnAl_2O_4$:Tb^{3+} (3 mol %) nanophosphor].

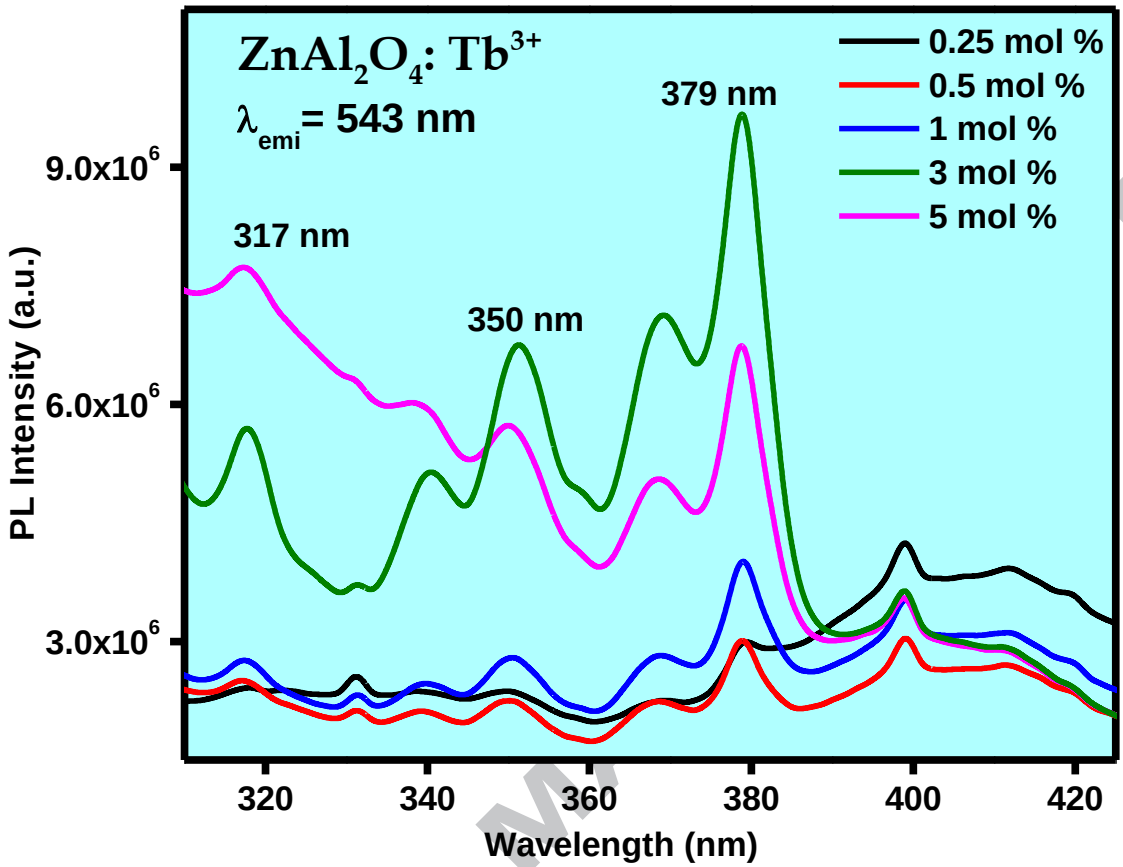

Fig.11. Excitation spectra of $ZnAl_2O_4$: Tb^{3+} (0.25-5 mol %) nanophosphor at λ_{Emi} = 543 nm.

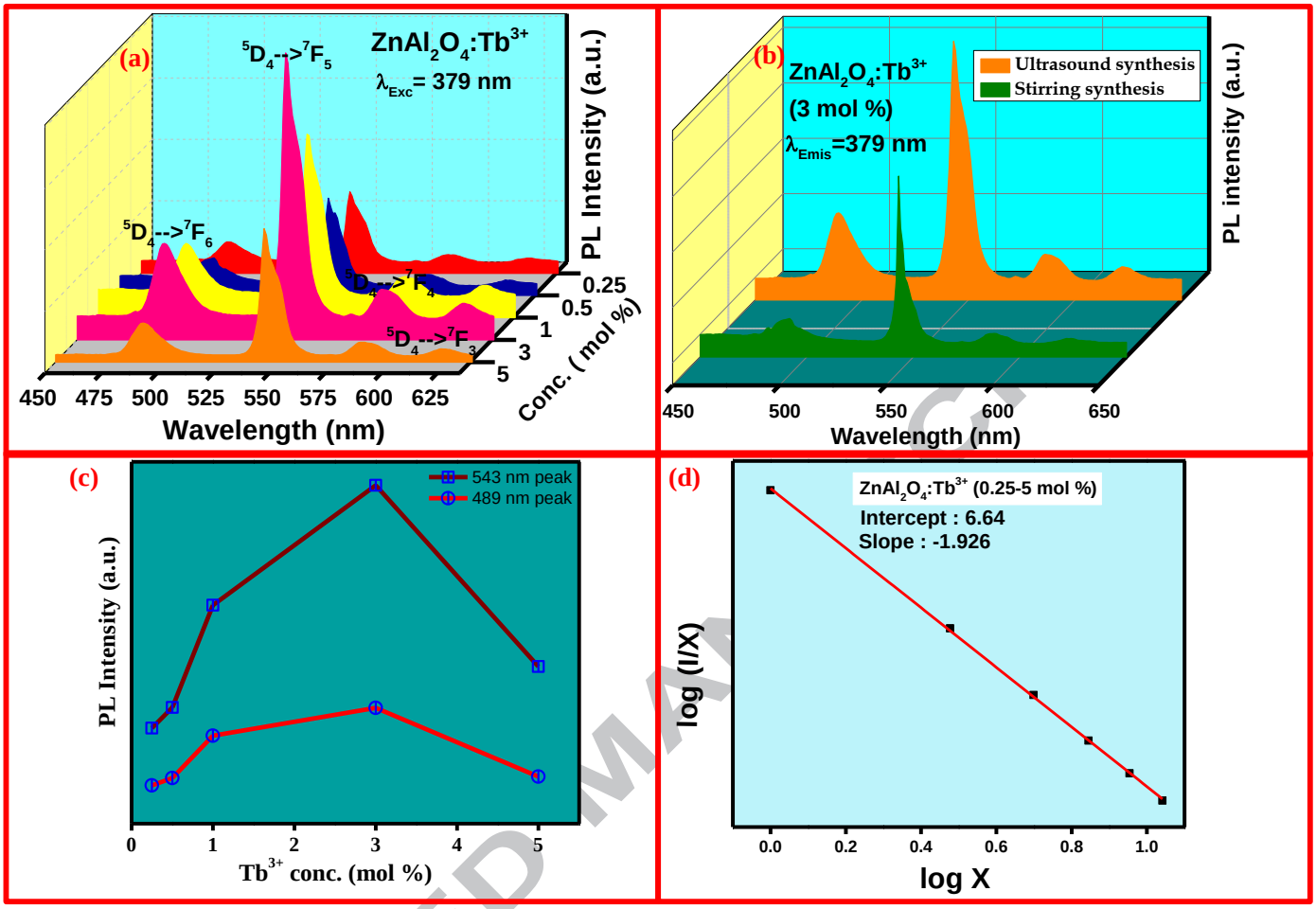

Fig.12 (a) Emission spectra of $ZnAl_2O_4$: Tb^{3+} (0.25 - 5 mol %) nanophosphor, (b) Emission spectra of $ZnAl_2O_4$: Tb^{3+} (3 mol %) nanophosphor with and without ultrasound irradiation, (c) Variation of PL intensity with concentration of Tb^{3+} ions and (d) Logarithmic plot of (x) V/s (I/x).

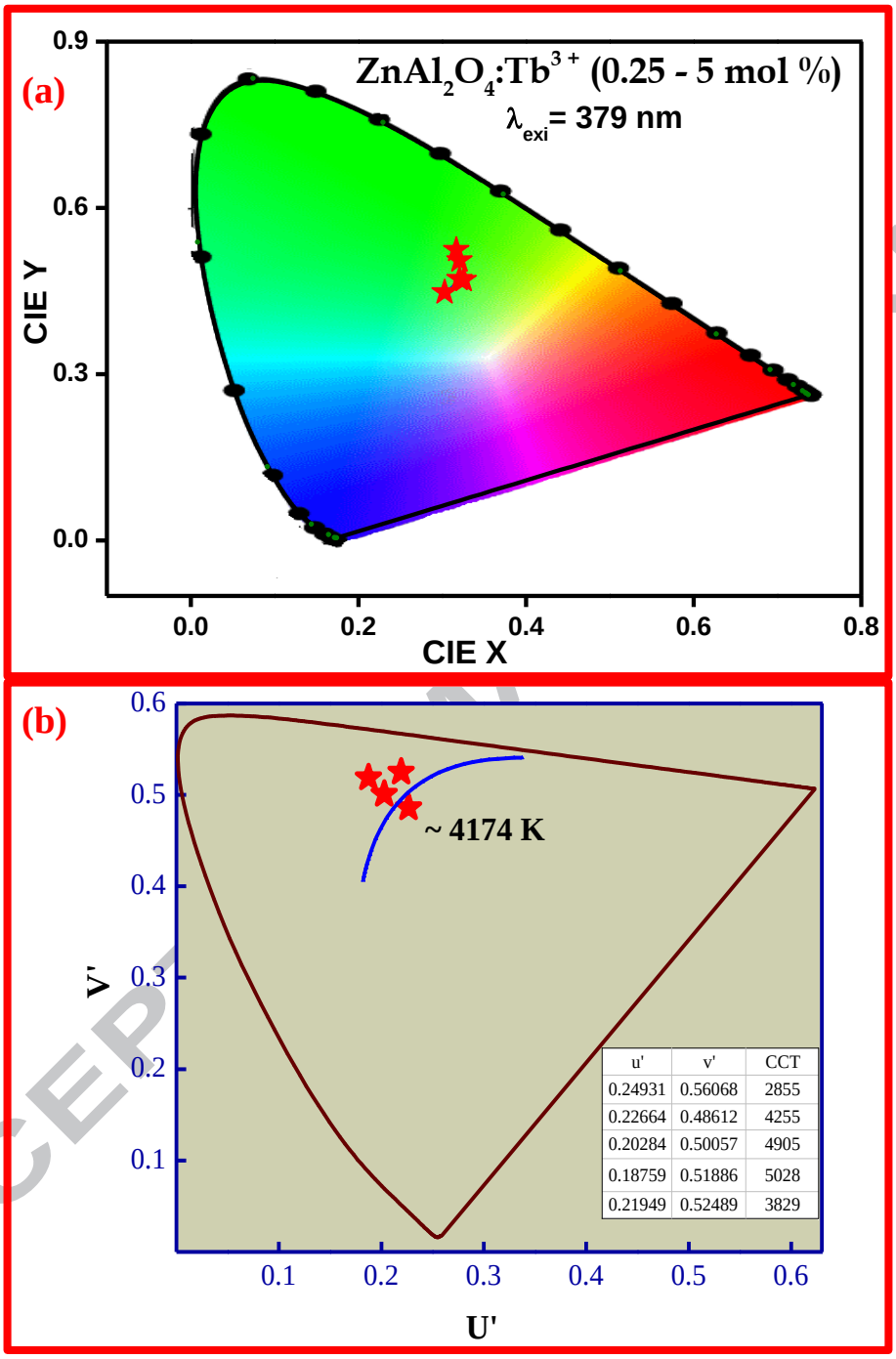

Fig.13 (a) CIE and (b) CCT diagram of $ZnAl_2O_4$: Tb^{3+} (0.25 – 5 mol %) nanophosphor.

Table.1. Estimated average crystallite size and strain of $ZnAl_2O_4:Tb^{3+}$ (0.25-5 mol %) nanophosphor from PXRD and TEM analysis.

Tb^{3+} conc. (mol %)	**Average Crystallite Size (nm)**		**Strain (ε) x 10^{-4}**	**Average crystallite Size (nm) obtained from TEM**
	Scherrer's approach	**W- H plots**		
undoped	30	31	1.23	34
0.25	28	30	1.45	30
0.5	27	28	1.85	30
1	23	22	2.3	24
3	22	18	4.74	17 (Fig.S4)
5	14	14	5.64	17

Table.2.Rietveld refinement parameters of $ZnAl_2O_4:Tb^{3+}$ (3 mol %) nanophosphor.

Atoms	Oxidation State	Wyckoff Notation	Positional parameters			B_{iso}	Occupancy
			x	*y*	*z*		
Zn1/Cr	+2/+3	8a	0.1250	0.1250	0.1250	0.050	1
Al 1	+3	16d	0.5000	0.5000	0.5000	0.500	1
O 1	-2	32e	0.2639(2)	0.2639(2)	0.2639(2)	0.500	1

Crystal system = Cubic; ***Lattice parameter***, *a* = 8.0707(4) Å; ***Space group*** = *Fd-3*(227), ***Cell volume*** = 525.696(2) $Å^3$; $\boldsymbol{R}_{Factors}$; R_p = 2.21, $\boldsymbol{R}_{wp}$ = 2.84, χ^2 = 0.20, $\boldsymbol{R}_{Bragg}$ = 1.95, R_F = 2.07.

Bond length**:** Zn – O x 4 = 1.943(2) Å, Al – O x 6 = 1.9192 Å.

Table.3. Estimated kinetic parameters of $ZnAl_2O_4:Tb^{3+}$ (3 mol %) nanophosphor γ- irradiated in the dose range 0.1-6 kGy.

γ-dose (kGy)	T_m (^oC)	b(μ_g)	Activation energy E (eV)			Frequency factor s (Hz)		
			Chen	Grosweiner	Luschiks	Chen	Grosweiner	Luschiks
0.1	188	1(0.46)	0.640	0.657	0.690	$1.49x10^7$	$1.07x10^7$	$1.99x10^7$
0.25	193	1(0.42)	0.568	0.558	0.566	$1.17x10^7$	$1.93x10^7$	$1.28x10^7$
0.5	194	1(0.41)	0.542	0.555	0.541	$8.06x10^6$	$8.64x10^6$	$8.43x10^6$
1	195	1(0.43)	0.556	0.554	0.552	$5.26\ x10^7$	$5.00x10^7$	$5.87\ x10^7$
2	195	1(0.43)	0.566	0.565	0.556	$9.71x10^7$	$9.86x10^7$	$9.85\ x10^7$
3	196	1(0.44)	0.647	0.609	0.671	$3.81x10^7$	$3.27x10^7$	$3.36\ x10^7$
4	197	1(0.43)	0.554	0.551	0.540	$5.22x10^7$	$5.77x10^7$	$5.71\ x10^7$
5	197	1(0.50)	0.694	0.596	0.537	$2.94x10^7$	$2.20x10^7$	$2.53\ x10^7$
6	198	1(0.42)	0.559	0.556	0.551	$8.00x10^6$	$8.35x10^6$	$8.34x10^6$

Table.4. Judd-Ofelt intensity parameters (Ω_2, Ω_4), Emission peak wavelengths ($\lambda_p$in nm), radiative transition probability (A_T), calculated radiative (τ_{rad}) lifetime, branching ratio (β_R) and asymmetric ratio (A_{21}) of $ZnAl_2O_4:Tb^{3+}$ (0.25-5 mol %) nanophosphor (λ_{ex} = 379 nm).

$ZnAl_2O_4:Tb^{3+}$ conc. (mol %)	**Judd-Ofelt intensity parameters ($\times10^{-20}$ cm^2)**		**Emission peak wavelength λ_p in nm**	**A_T (s^{-1})**	**τ_{rad} (ms)**	**β_R**	**A_{21}**
	Ω_2	**Ω_4**					
0.25	6.23	1.08	549	50.7	17.3	0.9	0.25
0.5	6.48	1.24	543	56.8	20.3	0.9	0.69
1	6.70	1.45	544	53.9	25.2	0.99	0.67
3	6.99	1.89	544	60.7	14.7	0.9	0.40
5	7.2	2.01	543	58.5	27.4	0.9	0.21

Table.5.Photometric characteristics of $ZnAl_2O_4:Tb^{3+}$ (0.25-5 mol %) nanophosphor.

Tb^{3+} Concentration (mol %)	**X**	**Y**	**CP (%)**	**CCT (K)**
0.25	0.3259	0.4698	85	2855
0.5	0.3029	0.4474	84	4255
1	0.3207	0.4717	88	4905
3	0.3207	0.5053	90	5028
5	0.3170	0.5240	81	3829